Natural Hazards
and Earth System
Sciences
Discussions
Open Access
EGU

Interactions between precipitation, evapotranspiration and soil moisture-based indices to characterize drought with high-resolution remote sensing and land-surface model data.

Jaime Gaona[1,2], Pere Quintana-Seguí[2], María José Escorihuela[3], Aaron Boone[4], María Carmen Llasat [5]

5 [1]Instituto de Investigación en Agrobiotecnología, CIALE, Universidad de Salamanca, Villamayor-Salamanca, 37185, Spain.
[2]Hydrology and climate change, Observatori de l'Ebre (Universitat Ramon Llull - CSIC), Roquetes, 43520, Catalonia, Spain.
[3]IsardSAT, Parc Tecnologic Barcelona Activa, Barcelona, 08042, Catalonia, Spain.
[4]GMME/MOANA (Groupe de Météorologie à Moyenne Echelle), MOdélisation de l'Atmosphère Nuageuse et Analyse CNRM-GAME (URA CNRS & Météo-France), 42, Av. G. Coriolis, 31057, Toulouse Cedex 1, France.
10 [5]Applied physics department, Faculty of Physics, University of Barcelona, Barcelona, 08028, Catalonia, Spain.

Correspondence to: Jaime Gaona (jaimegaona@usal.es)

Abstract.

The Iberian Peninsula is prone to drought due to the high variability of the Mediterranean climate with severe consequences for drinking water supply, agriculture, hydropower, and ecosystems functioning. In view of the complexity and relevance of droughts
15 in this region, it is necessary to increase our understanding of the temporal interactions of precipitation, evapotranspiration and soil moisture that originate drought within the Ebro basin, in northeast Spain, as study region. Remote sensing and land-surface models provide high spatial and temporal resolution data to characterize evapotranspiration and soil moisture anomalies in detail. The increasing availability of these datasets has potential to overcome the lack of in-situ observations of evapotranspiration and soil moisture. In this study, remote sensing data of evapotranspiration from MOD16A2ET and soil moisture data from SMOS1km
20 as well as SURFEX-ISBA land-surface model data are used to calculate the EvapoTranspiration Deficit Index (ETDI) and the Soil Moisture Deficit Index (SMDI) for the period 2010-2017. The study compares the remote sensing time series of these ETDI and SMDI indices with the ones estimated using the land-surface model SURFEX-ISBA, including the Standardized Precipitation Index (SPI) computed at weekly scale. The study focuses on the analysis of the temporal lags between the indices to identify the synchronicity and memory of the anomalies between precipitation, evapotranspiration and soil moisture to interpret factors
25 involved in drought onset. Lag analysis results demonstrate the capabilities of the SPI, ETDI and SMDI drought indices to inform about the mechanisms of drought propagation at distinct levels of the land-atmosphere system. Relevant feedbacks both for antecedent and subsequent conditions are identified, with a preeminent role of evapotranspiration in the link between rainfall and soil moisture. Both remote sensing and land-surface model show capable to characterize drought events, with specific advantages and drawbacks of the remote sensing and land-surface model datasets. Results underline the value of analyzing drought with
30 dedicated indices, preferably at weekly scale, to better identify the quick self-intensifying and mitigating mechanisms governing drought, which are relevant for drought monitoring in semi-arid areas.

1 Introduction

Drought is a major natural hazard for the societies in semi-arid climates (Van Loon, 2015) which demands increasing levels of adaptation and resilience measure to guarantee water supply (Watts et al., 2012), particularly in water-stressed environments. Rain-
35 fed agriculture (Tigkas and Tsakiris, 2015), and even the enduring natural vegetation are very exposed to drought, especially under climate change, which has long-lasting implications to the local environment (Gudmundsson et al., 2014). Knowing that complex interactions take place in the land-atmosphere system under drought, the traditional meteorological or hydrologic approach may

overlook drought-relevant interactions between evapotranspiration and soil moisture (Teuling et al., 2013). This explains why modern drought monitoring combines evapotranspiration, soil moisture and even vegetation anomalies to track drought status,

40 such as the European Drought Indicator (Sepulcre-Cantó et al, 2012). Even though long-term anomalies of rainfall, evapotranspiration and soil moisture are regularly monitored and known to play a role in the recurrence of drought and heat waves (Zampieri et al., 2009; Dasari et al., 2014), often short-term anomalies are overlooked, especially regarding interactions of evapotranspiration and soil moisture.

45 Well-known drought indices such as the standardized precipitation index (SPI) (McKee, Doesken and Kleist, 1993) and the Palmer drought severity index (PDSI) (Palmer, 1965), primarily defined at the monthly scale, can lack detail to identify short-term anomalies of temperature, wind or radiation originating "flash droughts" (Otkin et al., 2013). Rain-fed agriculture and natural vegetation are particularly sensitive to quickly evolving droughts in specific moments of the growing season (Saini and Westgate, 1999), which subsequently generates evapotranspiration and soil moisture anomalies of short and long-term impact (Jimenez et

50 al., 2011). Recently, there is more interest on using drought indices with high temporal resolution for short-term drought monitoring, such as the SPI and other indices at the weekly scale (Otkin et al., 2015). Indices with this short-term time scale include the weekly-scale evapotranspiration deficit index (ETDI) and the soil moisture deficit index (SMDI) (Narasimhan & Srinivasan, 2005). The ETDI and SMDI indices are variable-specific enabling full characterization of anomalies at specific levels of the atmosphere-surface system. This is especially useful in the Mediterranean climates where not only rainfall anomalies originate

55 drought (Vicente-Serrano et al., 2004).

This study focuses in the Ebro basin, which is an important Mediterranean river basin of the Iberian Peninsula (IP). In view of the increase in the frequency of drought events (Sousa et al., 2011) and in the number of consecutive dry spells (Turco and Llasat, 2011) identified in the area, we can expect consequences in the long-term environmental state and the balance between water

60 availability and demands. Furthermore, being placed in a semi-arid climate where most of the rainfall evaporates (68%, Table 15, of "Libro blanco del agua" (MMA, 2000)), the Ebro basin represents an example of how important natural water demands are, particularly in the headwaters where runoff decrease due to reforestation (López-Moreno et al., 2014). Rainfed agriculture dominates the rest of un-forested areas and represents the other big consumer of water in the basin. However, despite the relevance of rainfed agriculture its analysis is often overshadowed by irrigation, the biggest anthropogenic demand in the basin (Hoerling et

65 al., 2012). Due to the importance of these water demands and others such as hydropower and energy, the Ebro River Basin Agency operates a dense hydrologic monitoring network, but the lack of dedicated soil moisture and evapotranspiration monitoring jeopardizes drought characterization (Seneviratne et al., 2010). Fortunately, the increasing availability of remote sensing (RS) products enables distributed, precise, and frequent monitoring of these coarsely observed variables (Martínez-Fernández et al., 2016).

70

Space agencies have released multiple RS products in the last decades facilitating the distributed analysis of drought (AghaKouchak et al., 2015). Optical spectrometry of the atmospheric (rainfall, temperature, water vapor) and surface (vegetation reflectance) variables have often been the basis for distributed characterization of drought indicators, but currently there are soil moisture datasets available from passive microwave sensors such as those from SMOS and SMAP missions (Kerr et al., 2010; Entekhabi et

75 al., 2010; respectively) or active microwave sensors such as ASCAT or Sentinel-1 (Bartalis et al., 2007; Hornacek et al., 2012; respectively), which are often combined for improved characteristics. In parallel to the RS missions, the development of processing techniques has improved the applicability of their derived data products (Wagner et al., 2007). This is the case of the high-resolution

soil moisture and evapotranspiration products SMOS1km (Merlin et al., 2013; Molero et al., 2016, Escorihuela and Quintana-Seguí., 2016; Escorihuela et al., 2018) and MOD16A2 (Mu et al., 2013) used in this study. Both RS products represent components

80 of the land-atmosphere system which are difficult to measure on the ground, particularly under extreme conditions such as drought (Miralles et al., 2019). To date, relatively few works have used satellite data for drought analysis in the IP (Vicente-Serrano, 2006; Scaini et al, 2015, Martínez-Fernández et al., 2016; Sánchez et al., 2016; Ribeiro et al., 2019), especially at the spatial and temporal resolution of this study (Pablos et al., 2019).

85 Another source of high-temporal and spatial resolution data is land-surface models (LSM). Used in atmospheric models to simulate the interactions between soil, vegetation and the atmosphere, LSMs evaluate the surface water and energy balances. LSMs initiated their development with one-layer models such as the TOPUP (Schultz et al., 1998) or the PROMET (Mauser and Schadlich, 1998) were developed. Avissar and Pielke (1989) inaugurated the mosaic approach, applying just one-layer models to the different fractions of land-use type. One of the mosaic models able to distinguish between soil evaporation and transpiration is the Météo-

90 France developed model SURFEX (Masson et al., 2013), which fed by the atmospheric analysis SAFRAN (Durand et al., 1999) uses the ISBA scheme for natural surfaces (Noilhan and Mahfouf, 1996). SURFEX has been improved to study the continental water cycle in applications such as SIM and SIM2 (Habets et al., 2008; Le Moigne et al., 2020), often in combination with the hydrologic model MODCOU (Ledoux et al., 1989). The modelling chain called SASER (SAFRAN-SURFEX-Eaudyssée-RAPID) used in this study has been applied to Spain before (Barella-Ortiz and Quintana-Seguí., 2019; Quintana-Seguí et al, 2020) and

95 gives the values required for SPI and SMDI.

This study aims at evaluating the suitability of high-resolution RS (SMOS1km and MOD16A2) and LSM (SURFEX-ISBA) data generating rainfall (SPI), soil moisture (SMDI) and evapotranspiration (ETDI) drought indices to better understand the mechanisms behind the temporal evolution of drought in semi-arid climates. The study evaluates the advantage of the barely explored weekly

100 temporal scale to capture the short-term anomalies of evaporation and soil moisture decisive to drought in semi-arid areas. The study has an agricultural scope focused on drought of rain-fed environments given its importance on the land-atmospheric feedbacks (Herrera-Estrada et al., 2017) and to the regional socioeconomic sustainability.

2 Study area

The study area is the Ebro basin, located in the north-east of the Iberian Peninsula (IP). Placed in between Atlantic and

105 Mediterranean climatic influences, the vast area (85534 km2) of the basin (Fig. 1a) has a complex topography (Fig. 1c) which defines a wide range of climatic conditions (Fig. 1d) of distinct spatial and temporal patterns of precipitation, evapotranspiration and soil moisture. The northern border has humid cool climates typical of the Atlantic-exposed Cantabric coastline, while the southeast border enjoys a warm Mediterranean climate. The southwest and north-eastern border are dominated by the Iberian and Pyrenees mountains which together with the Cantabric and Mediterranean ranges restrict the oceanic influence on the central part

110 of the basin. Soil types (e.g. gypsum, limestones) intensify the aridity of certain areas of the basin (Fig. 1b). The combination of semi-arid climatic conditions and unfavorable soil types to vegetation development determine extreme regimes of rainfall, soil moisture and evapotranspiration, prone to drought. The basin is densely populated and supplies a wide range of water demands, especially for agriculture and energy. The vast network of irrigated areas, located mostly in the arid central depression, is vulnerable to hydrological drought risks.

115

3 Data

3.1 Land-Surface Model Data

SURFEX, the land-surface modelling platform originally developed and currently maintained by Météo-France (Mason et al., 2013; Le Moigne, 2020), has been chosen to perform the LSM model simulation used in this study. Simulation for the IP and

120 Balearic Islands developed within the HUMID project have 5km spatial resolution, with the forcing provided by the Iberian application (Quintana-Seguí et al., 2008; 2016; 2017) of the SAFRAN meteorological analysis system (Durand et al, 1999). This is a modelling chain whose offline mode operates using the atmospheric forcing of SAFRAN to feed the LSM SURFEX-ISBA and simulate even the hydrology with Eaudyssée-RAPID (David et al. 2011).

125 ISBA (Noilhan and Mahouf, 1996) is the SURFEX module in charge of simulating natural surfaces. There are different versions of ISBA, in this study we have use diffusion version (ISBA-DIF; Boone, 1999; Decharme et al., 2011), which performs better in the study area than the simpler 3-layer force restore version (Quintana-Seguí et al., 2020). In this version of ISBA, the LAI has a prescribed annual cycle (constant every year), which may limit the ability of the model to reproduce the long-term effects of drought on vegetation. The model simulates the soil column, but it is unable to simulate groundwater, which despite its impact on

130 soil moisture memory is fortunately not very relevant in the Ebro basin. SURFEX-ISBA requires additional physiographic information that is incorporated from the ECOCLIMAP II land cover database (Faroux et al., 2013) which includes topographic, soil and land cover information at high-resolution.

The available SAFRAN forcing data allows us to simulate the period 1979-2017, but the period used for this study is restricted by

135 RS data due to the relatively short length of SMOS data (2010-present) compared to the model. To ensure the comparability of RS-based and LSM-based drought indices, the study period is 2010-2017, for which both RS and LSM data is available. To ensure that the RS and the LSM soil moisture is comparable, we have averaged three first soil layers of the model according to their discretization in the first 5 cm of the soil (1, 3 and 10 cm of depth respectively). The simulation is performed using a regular 5 km resolution grid based on a custom Lambert Conical Conformal projection.

140 ### 3.2 Remote Sensing Data

3.2.2 Evapotranspiration

To evaluate evapotranspiration, barely measured in the ground and not directly measurable from space, we adopt a product based on multiple evaporation-related variables observed by MODIS (Moderate Resolution Imaging Spectroradiometer on NASA's Terra satellite): the MOD16A2 dataset. This is a level 4 product providing 8-day evapotranspiration (ET) and potential evapotranspiration

145 (PET) based on daily meteorological forcing and 8-day RS data of vegetation dynamics from MODIS (Mu et al., 2013). The datasets of MOD16A2 are published in a sinusoidal projection at a resolution of 500 m (Running et al., 2017). In this study we have re-projected and interpolated all RS products to the same 5 km grid that the LSM simulations use. After the re-gridding step, the temporal step of the datasets is rearranged from the original 8-day accumulation period to a more practical 7-day accumulation period which is more suitable for weekly analysis. Values are linearly weighted depending on their contribution to each week-year

150 for the 52 weeks of a year. We also calculate the monthly means of the evapotranspiration product in order to evaluate the impact of the time resolution on drought recognition. The formatting of MOD16A2 datasets requires evaluation of the quality control flags

(ET_QC), given that areas of the Pyrenees show missing data. Only the classes classified as good an optimal in the ET_QC flags are accepted as data for our study.

3.2.3 Surface Soil Moisture

155 In view of the relatively few years of data currently available from the Soil Moisture Active Passive mission SMAP (Entekhabi et al., 2010), the study adopts SMOS data (Kerr et al., 2010), in particular, the SMOS1km dataset (Merlin et al., 2013). This dataset downscales the original coarse resolution SMOS data using the Disaggregation based on Physical And Theoretical scale Change algorithm DISPATCH (Merlin et al., 2012) / C4DIS (Molero et al., 2016) algorithm. The algorithm enables the downscaling of the 40 km resolution of the SMOS soil moisture data available from 2010 into 1 km resolution using two products at 1 km resolution

160 from MODIS, the NDVI and LST, and an elevation map at the same resolution. Precisely because the scale of interest to study relevant interactions to droughts is the weekly scale, the data is primarily used at weekly scale. The 2010-2017 dataset presents frequent gaps in the mountainous areas of the Pyrenees. In order to fill the gaps, we apply temporal interpolation. These data are also spatially aggregated and reprojected to the same grid as the LSM model.

4 Methods

165 ### 4.1 Drought indices

Drought indices allow quantifying several aspects of drought, like the magnitude and duration, and may also focus on particular variables depending on the scope of interest (i.e. precipitation, soil moisture, aridity…etc.). In view of the convenience to combine several indicators to describe the most about the drought evolution and our focus on rain-fed environments, we adopt the use of the Standardized Precipitation Index (SPI) (McKee, Doesken and Kleist, 1993), the Evapotranspiration Deficit Index (ETDI) and

170 the Soil Moisture Deficit Index (SMDI) (Narasimhan and Srinivasan, 2005). Using these three indices, the study aims to investigate the interaction between the two main water fluxes (rainfall and evapotranspiration) and the main storage (soil moisture) involved in the water balance of the land-atmosphere system. The aggregation periods of the SPI index inform about the different responding times of rainfall, soil moisture, streamflow, and groundwater anomalies. By evaluating the evolution of these indices along with their interactions, this study aims to characterize drought mechanisms in the Ebro basin. In this study, the indices have been

175 computed using gridded datasets, thus, generating a time series for each grid point.

4.1.1 SPI

The Standardized Precipitation Index (SPI) (McKee, Doesken and Kleist, 1993) is an index of precipitation anomalies, which is calculated by transforming the accumulated precipitation from its original distribution (usually gamma or Pearson Type III) to the normal distribution with zero mean and unit standard deviation. As a result, we obtain a time series that shows, for each time step,

180 the departure from the expected value in terms of standard deviations. The calculation of the index is usually done based on monthly time series of rainfall, aggregated over multiple accumulation periods, typically at 3, 6, 12 months. However, SPI can also be calculated on a weekly basis, provided that the accumulation periods are at least 4 weeks (1 month). In this way, this study uses the notation SPIm-i to denote the SPI at monthly scale with accumulation period of i months and the SPIw-i to denote the weekly SPI with accumulation period of i weeks. Using SAFRAN data, we adopt the non-parametric methodology proposed by Farahmand

185 and Aghakouchak (2015) to calculate the SPI on a monthly and weekly basis using the multi-month accumulation of 1, 3, 6 and 12 months suitable for rainfall, soil moisture, streamflow and groundwater evaluation.

4.1.2 ETDI

The second index incorporated to the analysis is the EvapoTranspiration Deficit Index (*ETDI*) defined by Narasimhan and Srinivasan (2005). The first step for calculating this index implies defining the water stress ratio (*WS*) for each week, which is the

190 difference between potential evapotranspiration (PET) and actual evapotranspiration (AET) divided by PET. Then the Water Stress Anomaly (WSA) is computed as follows:

$$WSA_{i,j} = \frac{MWS_j - WS_{i,j}}{MWS_j - \min WS_j} x100, \quad if \; WS_{i,j} \leq MWS_j$$

$$WSA_{i,j} = \frac{MWS_j - WS_{i,j}}{\max WS_j - MWS_j} x100, \quad if \; WS_{i,j} > MWS_j \tag{1}$$

where *j* denotes the week of the year (1 <= *j* <= 52) and *i* denotes the year. $WS_{i,j}$ is the water stress of the week *j* of the year *i*.

195 MWS_j is the median WS for the week *j* of the year, *minWSj* corresponds to the minimum and *maxWSj* the maximum. This process removes the seasonality of the time series. *WSA* ranges from -100 (maximum water stress) to 100 (minimum water stress). The WSA is accumulated over time to define the *ETDI* as in the following equation:

$$ETDI_j = 0.5 \; ETDI_{j-1} + \frac{WSA_j}{50} \tag{2}$$

To define a range between -4 and 4 for the index, ETDI of value -4 must correspond to WSA of value -100 and ETDI of value 4

200 to WSA of value 100. This range adjustment determines the coefficients 0.5 and the divisor 50 of Eq. (2). In this way, ETDI becomes a non-seasonal index suitable for comparing time series of diverse climatic characteristics.

Monthly values of the ETDI are calculated by computing the average of the weekly values of the corresponding month. In this study we calculate the ETDI using potential and actual evapotranspiration provided by MOD16A2. We have also calculated it using the SURFEX-ISBA simulated AET and PET. By default, SURFEX-ISBA does not calculate potential evapotranspiration. In

205 order to do so, we have modified the source code to set soil moisture permanently at field capacity and have run a simulation with this modification. The resulting evapotranspiration corresponds to the potential one.

4.1.3 SMDI

The third index incorporated to the analysis is the Soil Moisture Deficit Index (*SMDI*) also defined by Narasimhan and Srinivasan (2005). The sequence to calculate this index follows the same procedure of the *ETDI*. We first calculate a weekly soil moisture

210 deficit as follows:

$$SD_{i,j} = \frac{SW_{i,j} - MSW_j}{MSW_j - minSW_j} x100, \quad if \; SW_{i,j} \leq MSW_j$$

$$SD_{i,j} = \frac{SW_{i,j} - MSW_j}{maxSW_j - MSW_j} x100, \quad if \; SW_{i,j} > MSW_j \tag{3}$$

Then, the time series of *SMDI* is generated accumulating *SD*:

$$SMDI_j = 0.5 \; SMDI_{j-1} + \frac{SD_j}{50} \tag{4}$$

215 *SMDI* also ranges between -4 and 4, respectively corresponding to extremely dry and very wet soil moisture conditions. The *SMDI*, similarly to the *ETDI*, becomes a non-seasonal index able to compare time series of diverse climatic characteristics at different soil depths. In this study we have calculate the SMDI using SMOS1km surface soil moisture data and SURFEX-ISBA simulated

surface soil moisture data. In the case of SURFEX-ISBA, we have calculated the weighted averages of the first two layers of the soil, which corresponds to the first 5 cm of the soil.

4.2 Analysis of interaction between the indices

4.2.1 Correlation between the indices

To evaluate the similarity between the series of the drought indices (SPI, ETDI and SMDI) we use a variant of the procedure applied by Barella-Ortiz and Quintana-Seguí (2019) and Quintana-Seguí et al. (2020), based on Barker et al. (2015). The method consists of computing the correlation between each pair of series of these three drought indices (e.g. SPIw-i and ETDIw and SMDIw); where *i* is the accumulation period, which varies from 4 weeks (1 month) to 52 weeks (1 year).

4.2.2 Temporal lag-analysis of the indices:

Following the correlation analysis between the series, we perform a lag-analysis of the correlation of the pairs of drought indices at weekly scale, introducing lags from -104 weeks to +104 weeks. We compare the ETDIw and SMDIw with the SPIw-i (being the period of accumulation for the SPIw-i= 4, 13, 26 and 52 weeks, equivalent to the SPIm-1, SPIm-3, SPIm-6, SPIm-12 months), as well as the ETDIw in relation to the SMDIw. The purpose of this analysis is to diagnose the reciprocity and memory in the interaction between rainfall and evapotranspiration, and rainfall and surface soil moisture. The relative abundance of positive over negative lags (and viceversa) provides information about the asymmetry of the interaction between the indices (precedence and delay). Negative lags refer to leading times of ETDIw and SMDIw in respect of SPIw-i (e.g. lag - 104, left side of the time bar) while positive ones (e.g. lag +104) represent lag times when SPIw-i precedes ETDIw and SMDIw (e.g. lag +104, right side of the time bar). The number of consecutive weeks of positive of negative lags with the increasing period of aggregation of the SPIw-i can inform about the memory of the interactions. For each time lag it is indicated the percentage of the basin affected by non-significant / significant correlation values (Grey / coloured scales of bars in Figs. 3-7). Positive /negative correlations indicate a direct / indirect relationship (red /blue bars in Figs. 3-7).

5 Results

5.1 Correlation between indices: Monthly scale in comparison to the weekly scale

The first two aims of the study are to evaluate the suitability of SPI, ETDI and SMDI indices to characterize the main anomalies in water exchanges of the land-atmosphere system and to evaluate the suitability of adopting the weekly scale for the analysis of drought indices compared to the use of the monthly scale. Regarding the first, results shown in Fig. 2 indicate a general agreement of the SPI, ETDI and SMDI indices (either computed at monthly or weekly scale) on the major events of dry and wet anomalies of the period 2010-2017. The dry period of 2011-2012 and the wet period from the end of 2012 to 2015 were properly depicted. However, we identified differences, especially in the case of the SMDI. This index tends to show a generally lower variability when calculated with the LSM compared to the other indices. RS results of SMDI differ from the other indices during the start of 2010 due to the uncertainties during the test period of SMOS mission. The left column of Fig. 2 shows the monthly SPIm-i and the monthly averaged ETDIm and SMDIm. Correlations between SPI-i and ETDI / SMDI are calculated at the monthly (Table 1, left columns) and at the weekly scales (right columns) for both RS and LSM data (where i= 4, 13, 26 and 52 weeks of aggregation, equivalent to 1, 3, 6 and 12 months). We test the significance of the correlations (p-value < 0.05) between indices for two subsets:

the entire period (2010-2017) and a subset of dry periods (i.e., when SPI<0, ETDI<0, SMDI<0). Then, we compare the observed (RS) and simulated (LSM) estimates of the indices to explore differences between data sources. RS and LSM ETDIm and SMDIm indices are moderately correlated (barely over 0.5, significant). Table 1 reports a value of r=0.58 (significant) between ETDIm RS

255 and SMDIm RS which is significantly higher than the r=0.32 between ETDIm LSM and SMDIm LSM. In general, despite the resemblance of RS and LSM series of ETDI and SMDI shown in Fig. 2, these two series differ. There is higher agreement between the RS and the LSM estimates of ETDIm (r = 0.77, significant) than between RS and LSM ones of SMDIm (r = 0.27).

Table 1 also reveals differences in the moderate correlation of the SPIm-i with the ETDI and the SMDI of different temporal

260 aggregations (i=1,3,6,12 months of SPIm-i accumulation) as well as between their RS and LSM versions. Correlation between SPIm and ETDIm RS increases with the aggregation period of the SPIm (r = 0.39, 0.62, 0.72, 0.81 respectively for SPIm-1, SPIm-3, SPIm-6, SPIm-12) while correlations of SPIm with ETDI LSM peak at SPIm-3 (r=0.8) and remain high for SPIm-6 (r=0.78) and SPIm-12 (r=0.71). The correlations between SPIm-i and SMDI RS show moderate correlation ranging from the SPIm-1 (r=0.42) to the maximum value of the SPIm-12 (r=0.63). SMDIm LSM exhibits a decreasing correlation pattern with the increasing

265 aggregation of the SPIm from SPIm-3 to SPIm-12 (r=0.45, 0.31, 0.3, 0.24 respectively for SPIm-1, SPIm-3, SPIm-6 and SPIm-12). Remarkably, correlations of LSM SPIm - SMDIm are lower than their RS pairs, which suggest data uncertainties in RS and LSM, as reported by Barella-Ortiz and Quintana-Seguí (2019) and by Quintana-Seguí et al. (2020)).
The monthly correlation analysis is additionally conducted for the subsets of dry periods (those of negative sign of the SPIm, ETDIm and SMDIm). Using the dry subset primarily decreases all correlations. Compared to the whole-time series correlations,

270 the RS ETDIm – SMDIm values decrease a bit while LSM ones increase a bit. Also, the SPIm-i – ETDIm /SMDIm correlations noticeably decline. Despite losing correlation and significance there is still an increase of correlations with the longer aggregation periods as observed in the whole series analysis.

Fig. 2 provides an overview of the effect of adopting the weekly scale (right column) instead of the monthly scale (left column).

275 The weekly scale substantially improves the temporal resolution of the plots. Subplots of SPI-i (a to d), ETDI (e) and SMDI (f) show how the weekly scale accurately reproduces the magnitude, tendency and duration of the monthly-scale anomalies, while the increase in temporal resolution additionally captures quick changes. Graphically, we noticed that the aggregation period applied to the SPI prevents from increasing the resolution of the weekly compared to the monthly scale, while the weekly scale strongly increases the ETDI and SMDI resolution (Fig. 2 e_2 and f_2).

280

The right columns of Table 1 indicate the correlations between indices at weekly scale compared to those at monthly scale, (the 'w' sub-index of ETDIw / SMDIw / SPIw denotes the weekly scale). There is an overall decrease of correlations at the weekly scale compared to the monthly scale, accentuated with the increasing period of aggregation (from SPIw-3 to SPIw-12). Correlations increase a bit compared to the monthly scale at the lowest period of aggregation of SPIw-i, especially for the ETDI (from r=0.39

285 to 0.57 / r=0.51 to 0.68 in SPIw-1 - SMDIw RS / LSM). For both RS and LSM data, the weekly scale lowers the correlation values of the SPIw-i with the SMDIw more than those with the ETDIw. Within the dry-period subset, all the correlations decrease too. The weekly scale lowers correlations due to the increase of variability of the weekly time series compared to the monthly ones but enables capturing the increasing complexity of interactions at shorter time scales.
Therefore, since quick shifts (Fig. 2 e_1 and f_1) are of great interest for drought analysis, we consider the weekly scale as the most

290 convenient for the lag analysis of next section. This decision benefits comparing drought indices at their highest temporal definition, which for the ETDI and SMDI indices is natively the weekly scale and for the SPI can be easily applied.

5.2 Temporal lag analysis:

The analysis of correlations between the temporally lagged time series provides valuable insight on how the indices interact with each other (e.g., in terms of reciprocity) and about the memory periods of one variable into the other (synchronicity). Plots of the

295   fraction of the area affected by each correlation level (from -1 to 1 in steps of r=0.2) for each lag period are shown in Figures 3 - 7. It is anticipated that the three evaluated indices will agree the most in a narrow range around lag = 0 (no lag) and that their correlation fades away progressively for the increasing lag periods beyond the scale of the propagation of drought.

5.2.1 Lag analysis SPI-ETDI

RS

300   The lag analysis of SPIw – ETDIw and SPIw – SMDIw shown in Fig. 3 - 6, aims at diagnosing the reciprocity, synchronicity and memory in the interaction between rainfall and evapotranspiration, and rainfall and surface soil moisture. Each subplot of Fig. 3 to 6 shows the correlation between the ETDIw and SMDIw indices with the SPIw-i index calculated for different aggregation periods (-$\underline{i}$) at the week scale: the SPIw-4, SPIw-13, SPIw-26 and SPIw-52 which are the equivalents of SPI-1, SPI-3, SPI-6 and SPI-12 at monthly scale. Negative lags refer to leading times of ETDIw and SMDIw in respect of SPIw-i (e.g., lag - 104, left side

305   of the time bar) while positive ones (e.g. lag +104) represent lag times when SPIw-i precedes ETDIw and SMDIw (e.g., lag +104, right side of the time bar).

In the case of the ETDIw – SPIw-i analysis based on the RS data, there is a remarkable cluster of positive correlations in the short term (indicated with the tag 'ST$_1$' (Short-Term) over the subplots of Fig. 3). This 'ST$_1$' cluster show relevant fractions of the basin

310   affected by significant moderate (0.4-0.6) values of correlation, particularly in the first weeks of the positive range of lags (from lag 0 to +4) (Fig. 3). The cluster lasts more with the increasing period of aggregation (Fig. 3 a) to d)) eventually becoming merged with the mid-term clusters. In view of subplots Fig. 3 a) to d), the 'ST$_1$' cluster extends from lag -13 to 4 in the case of SPIw-4, from lag -13 to + 13 in the case of SPIw-13, and once merged with 'MT$_1$' from -26 to +26 in the case of SPIw-26 and from -26 to +39 for the SPIw-52. The mid-term cluster 'MT$_1$', originally indicating a period of correlation of ETDIw preceding SPIw-i from

315   4 to 13 weeks of aggregation, displays moderate to low but significant values of correlation (from 0.2 to 0.4) from lag -36 to -13. The merging of the cluster 'ST$_1$' and 'MT$_1$' decreases the asymmetry defining the leading role of ETDIw on SPIw-i. The initially asymmetric interaction of ETDIw – SPIw-i mostly located in the negative range of lags ('ST$_1$' and 'MT$_1$' shown between lag -30 and +10 for the SPIw-4 and SPI-13 cases) propagates and dampens towards the positive range of lags with the increasing aggregation. The dampening eventually shifts the interaction of ETDIw to SPIw-i from preceding to delayed (at 26 and 52 weeks

320   of aggregation, the clusters of significant positive correlations are mostly within the positive range of lags, especially in Fig. 3 d). Conversely, the loss of asymmetry due to the increasing aggregation translates into an increase of the duration of the cluster as well as of the fraction of the basin significantly affected by correlations. There is an additional cluster of positive correlations 'LT$_1$' past the year and half (lags +78 to +104), particularly noticeable at SPIw-13 and -26. Blue bars in Fig. 3 indicate negative correlations for the relationship ETDIw – SPIw-i dominating the long-term between evapotranspiration and rainfall anomalies.

325   There is a couple of clusters around lag +42 (tagged with 'LT$_2$') and around lag +104 ('LT$_4$'), slightly significant, that similarly to the positive correlations, increased in duration and magnitude with the increase of the aggregation period of the SPI, particularly for SPIw-26 and 52 (Fig. 3c - d).

LSM

330   Results from the LSM SURFEX-ISBA (Fig. 4) show a less lasting and more concentrated cluster of significant positive correlations around lag 0 ('ST_1' tagged in Fig. 4) than those observed in the RS results (Fig. 3). This result implies there is more synchronicity between SPI and ETDI in LSM data than in the RS data. Furthermore, the LSM provides higher magnitudes of the significant positive correlations of ETDIw – SPIw-i of ST_1 than RS results. Similarly to RS data, the duration of the highly correlated period 'ST_1' extends with the increasing aggregation of the SPIw-i (Fig. 4 a to d), eventually causing the merge of clusters 'ST_1' and

335   'MT_1'. The initial asymmetry of the positive correlations towards the negative range of lags is due to the cluster 'MT_1' placed around lag -26 and cluster 'LT_1' (Fig. 4 a and b). In the SPIw-26 and SPIw-52 cases (Fig. 4 c and d) 'LT_1' disappears, and the 'ST_1' merges with 'MT_1', shifting the initial asymmetry dominating the negative range of lags towards the positive range. Thus, the precedence of ETDIw with SPIw-i prevalent in the period of aggregation of 4 and 13 weeks translates into a precedence of SPIw-i with ETDIw in SPIw-26 and -52. The initial asymmetry of the cluster 'ST_1' – 'MT_1' is lower in LSM results (Fig. 4) than

340   in RS results (Fig. 3) due to the lower magnitude of 'MT_1'. The additional cluster of positive correlations 'LT_3' past the year and half range of positive lags (lags +78 to +104) in LSM results (Fig. 4a to c) concurs that of RS results (Fig. 3a to c). LSM results (Fig. 4) show a few more clusters of negative correlations ETDIw – SPIw-i but of lower magnitude than those of RS ones (Fig. 3). These significant clusters merge with the increasing aggregation period 'LT_4 – LT_5', which agrees with 'LT_2' shown in RS at the 26- and 52-weeks period of aggregation of SPIw-i. LSM results further include a cluster of significant negative correlations values

345   in the lead time range (cluster 'LT_2') that is absent in RS results (Fig. 4 vs. Fig. 3). The agreement between LSM and RS results confirm the asymmetrical interaction between ETDIw and SPIw-i. The asymmetry suggests certain prevalence of the precedence of positive correlations of ETDIw with SPIw-i in the short term (from the month to the seasonal scale) while points to some delayed response of ETDIw to SPIw-i in the negative correlations in the mid to long-term (from seasonal to interannual scale). The LSM results tend to amplify the magnitude and the area affected by positive correlations compared to the RS dataset. The asymmetry of

350   the ETDIw – SPIw-i becomes also more shifted towards the positive range of lags with the increasing aggregation period in LSM than in RS results.

5.2.2 Lag analysis SPI-SMDI

RS

   The interaction of SPIw-i with SMDIw for the RS dataset is not as strong as it was with ETDIw (Fig 5 and 6 vs. Fig. 3 and 4).

355   Both the correlation values and the significant fraction of the basin affected by them are lower than in the case of the ETDIw. Conversely to the ETDIW, the significant positive correlations around lag 0 ('ST_1') are symmetrical. In view of this, the SMDIw tends to experience the effect of the preceding conditions of the SPIw-i more than influencing those of the SPIw-i. The increasing period of aggregation of the SPIw-13, -26 and -52 widens and lags the short-term influence of the SPIw-i on the SMDIw ('ST_1') into a short to mid-term influence ('ST_1-MT_1'). This widened cluster of positive correlations stays almost entirely in the positive

360   range of lags, which differs from that of the ETDIw where the 'ST_1-MT_1' cluster extended both in positive and negative ranges of the lags (Fig. 5 compared to Fig. 3 to 4). The leading range of lags (from lag -104 to lag 0) does not show relevant clusters of significant correlation at all, neither on the mid nor in the long term. Negative correlations of the SMDIw – SPIw-i interaction only occasionally stand up at a small cluster ('LT_1', Fig. 5 b - d) in the positive range of lags (when SPIw-i precedes SMDIw). The smoothing effect of the aggregation period of SPIw-i increases the delay of this 'LT_1' cluster but differently from in ETDIw cases,

365   the magnitude of the significant negative correlations decline.

LSM

The LSM results for the SMDIw – SPIw-i relationship depict strongly dampened patterns of significant correlation between SMDIw and the SPIw-I compared to those of RS SMDIw – SPIw-i or ETDIw – SPIw-i. Only the 'ST$_1$'cluster is noticeable around lag 0. The increase of the aggregation period does not favor its permanence as relevant cluster beyond the SPIw-4. The cause can be the generalized low values of both non-significant and significant correlations obtained for these estimates of LSM SURFEX-ISBA which may indicate the difficulties of the LSM to describe the response of the surface soil moisture (the SMDI index) to the atmospheric forcing (the SPI index) that we saw in the RS dataset. The periods identified of short-term, mid-term and long-term influence of one SPIw-i in the SMDIw such as 'SP$_1$', 'MT$_1$', 'LT$_1$' cannot be recognized in Fig. 6 compared to Fig. 5. Therefore, the LSM results of the SPIw-i – SMDIw relationship strongly differ from the ones obtained from RS data and is a matter of debate in the discussion section.

5.2.3 Lag analysis ETDI-SMDI

RS

The remaining interaction in this analysis is the ETDI – SMDI. The results show a less asymmetric relationship between the ETDI and the SMDI compared to the ones between SPIw with ETDI and SMDI. The significant moderate positive correlation values (red bars in Fig. 7a) between lag 0 and +13 and from lag -10 to 0 indicate that the influence of the ETDI on the SMDI lasts longer than the one of the SMDI on the ETDI. The magnitude, though, express that SMDI moderately impacts the short-term conditions of the ETDI for about a month in comparison to the sole week the ETDI affects moderately those of SMDI. However, the highest correlations occur for the lag -1 when SMDI precedes ETDI in one week. Negative clusters 'MT$_1$, MT$_2$' at +/- 39 weeks suggest that the interaction between the indices goes beyond the seasonal scale commented above. However, the significance of all these mid to long-term clusters remain low.

LSM

The results of ETDI – SMDI interaction based on LSM data show less evident periods of interaction between the indices compared to the RS results. The expected strong correlation around lag 0 is largely diminished. The strongest cluster appears from lag -21 to -39 'MT$_1$' (Fig. 7b) when SMDI precedes ETDI. No notable negative clusters can be identified. Apart from the lack of agreement on the symmetry of the interaction between LSM and RS results (Fig. 7b vs. 7a), the notable cluster 'ST$_1$' in RS results is less relevant in LSM results. In view of the disparity between LSM and RS results we rise concerns about the accuracy of offline LSM simulations compared to the RS results, addressing them for discussion in the next section.

6 Discussion

Results require careful discussion regarding three main aspects: firstly, the effect of adopting the weekly scale for drought indices and analyses, secondly the meaning behind the complex interactions between drought indices and thirdly the comparison of RS and LSM as tools for high-resolution monitoring of drought. All comments refer to the results at a weekly scale.

6.1 Scales for drought monitoring in semiarid environments

Analyzing the differences in correlations between indices at monthly and weekly scales (Figure 2), we support the necessity of adopting the weekly scale to study lags between relevant variables driving drought processes, because the monthly scale preferred

for drought assessment from a hydrological perspective may overlook the quick response of the land-atmosphere interactions. The clusters of moderate to high correlation between indices mostly occur within the first month preceding or following an anomaly (Figs. 3-7), particularly in the short to very short-term. Apart from the tendency of high correlations to peak and plunge in the interval of a few weeks, the information about its delay or precedence can only be observed when the weekly scale is adopted. Our

405 results showing soil moisture response to rainfall (-5 to 5 weeks) and evapotranspiration (-10 to 5 weeks) anomalies in the matter of weeks are consistent with previous works showing soil moisture echoing rainfall anomalies in a range from days to weeks (Scaini et al., 2015; Martínez-Fernández et al., 2016), but also when driven by evapotranspiration (Otkin et al., 2013). Therefore, in a basin exposed to the high-energy characteristics of semi-arid climates, the weekly scale increases the capability to diagnose quick and often disregarded interactions such as the short-term interactions of ETDI and SMDI on SPI, without losing resolution

410 in the identification of mid to long-term interactions. An additional aspect to bear in mind when shifting to the weekly scale for drought assessment is that the spatial resolution must increase accordingly. We identified that certain inputs of the LSM model (mainly the forcing dataset, which nominally has a resolution of 5 km, but which has a lower real resolution due to the spacing between meteorological stations) may undermine the resolution of LSM results compared to the ones from RS. This is a scale effect reported by Rodriguez-Iturbe et al. (2001), who warned that coarse resolution of the spatial characteristics increases the

415 temporal scale "at which the processes are effectively correlated". Therefore, lag analysis must compile datasets of appropriate spatial and temporal scales for their aims.

6.2 Interpretation of the interactions between drought indices

Adopting specific drought indices for rainfall, evapotranspiration and soil moisture allows to explore the interactions between variables of different levels of the land-atmosphere system. Fig. 8 a) and 8 b) graphically summarizes the annual mode of

420 interactions. In the short to mid-term, both the ETDI and SMDI interactions with SPI concur on having moderate significance, with only a few negative and positive low interactions in the mid to long term. Positive correlations around lag=0 of the ETDI and SMDI with SPI indicate direct precedent dependence of the indices, which means ETDI and SMDI correlate positively (negatively) to positive (negative) changes on the SPI. The short-term correlations after rainfalls for both ETDI and SMDI (lagged response of these indices to SPI) have immediate interpretation and was reported before in similar Iberian regions (Martínez-Fernandez et al.,

425 2016). Sustained dry or wet anomalies in both variables favored by positive correlation between indices are primarily restricted to a length of three seasons, while remain less probable beyond a year. The merging effect of the 'ST$_1$ – MT$_1$' clusters with the increase of the aggregation period implies that the reinforcing positive interaction of SPI-ETDI /SMDI can be identified easily at monthly or even seasonal scales. This also affects correlations beyond the year scale suggesting some multi-annual persistence of the positive reinforcing anomalies, nothing infrequent in Mediterranean climates.

430

The precedent influence of ETDI and SMDI on SPI (clusters of the negative range of lags) is weaker than the influence of SPI on subsequent ETDI and SMDI anomalies (lagged response). It is reasonable that the lagged response of evapotranspiration and soil moisture to rainfall is stronger and more long lasting than the precedent influence (Fig. 8 a). Nonetheless, the existence of precedent influence implies some reciprocity (feedback) between evapotranspiration and soil moisture with rainfalls. The precedent influence

435 period between the ETDI and SPI is stronger and of longer duration than the one of SMDI on SPI. This asymmetry suggests that ETDI, more than SMDI, has weekly to seasonal precedent influence on rainfall (Fig. 8b). We expected a longer period of positive correlations of SMDI influencing rainfalls, given the multiple reports of soil moisture inducing memory to the near-surface atmosphere (Manning et al., 2018). One reason that the ETDI shows longer influence on SPI than SMDI may be that ETDI from MOD16A2 is fed by the whole depth of soil moisture, while SMDI based on SMOS1km is limited to the top 5 centimeters of soil

Natural Hazards
and Earth System
Sciences
Discussions
Open Access
EGU

440 moisture, a very exposed soil level in semi-arid climates. Other reasons to this may be in the prevalence of maritime advection as main contributor to evapotranspiration in the IP (Gimeno et al., 2010), compared to the prevalence of local soil moisture recycling common in the continental areas of Europe (Bisselink and Dolman, 2008). The advective explanation is supported by the contrast between the few weeks of precedent influence of soil moisture on rainfall we observe in the Ebro basin and the up to 250 days of precedent influence of continental areas prone to soil moisture recycling (Rowntree and Bolton, 1983; Bisselink and Dolman,

445 2008). The complexity of soil moisture dynamics, which barely follow a cyclic interaction (Rodriguez-Iturbe et al., 1991), can represent an additional reason for a weaker relationship between the SMDI and SPI compared to the ETDI.

The sequence of the described precedent influences and lagged responses can suggest the existence of a reinforcing or self-intensification loop (Brubaker and Entekhabi, 1996), by which the precedent influence of positive (negative) anomalies of

450 evapotranspiration increasing (reducing) rainfall cascades into a lagged enhanced (depleted) response of evapotranspiration restarting the cycle (Fig. 8b). The weak precedence of soil moisture on rainfall compared to that of evapotranspiration expresses the limited power of the reinforcing soil moisture loop (based on rainfall recycling) to inhibit the self-intensification loop of evapotranspiration in semi-arid climates (upper sequence of Fig. 8c). This reason explains why droughts may eventually fail to terminate before heavy rainfall. However, the weakness of the soil moisture feedback may be partly due to working with surface

455 soil moisture instead of root zone soil moisture. In any case, since the precedent influence of evapotranspiration is stronger than the one of soil moisture, the reinforcing loop of evapotranspiration likely exceeds the inhibiting effect of soil moisture. This is in line with reports highlighting the power of evapotranspiration anomalies in drought generation (Otkin et al, 2013) and the prominence of evapotranspiration on the partitioning of energy during hydrometerological extremes (Seneviratne et al., 2006) such as during heat waves when high temperature and wind conditions enhance the impact of evapotranspiration. Another reason

460 supporting the dominance of evapotranspiration over soil moisture is that rainfall mostly transfers to evapotranspiration in semi-arid climates (Rodriguez-Iturbe et al., 2001), where the often-underestimated interception (Savenije et al., 2004) further increases evaporation at the expense of soil moisture. Eventually, the self-intensification loop may go beyond the interactions described here and alter the atmosphere (Miralles et al., 2019). However, we bear in mind that our results may oversimplify the causality since processes not analyzed in this study may also play a role.

465

Negative correlations when indices differ in sign (r<0 conditions, Fig. 8a) can be indicative of transitional periods of mid-seasons. The sharp shift from the cluster of short-term positive correlations to the cluster of mid- to long-term negative correlations suggests a limit in the persistence of the self-intensification mechanism. A physical interpretation of the shift may be related to the change in the dominance of the driving variable. The previous paragraph described the positive feedback mechanism driven by

470 evapotranspiration, but Brubaker and Entekhabi (1996) also described an inhibiting feedback mechanism of negative correlations between soil moisture and surface temperature when temperature is low. Given the direct link between evapotranspiration and temperature, the shift from positive to negative interactions beyond the semester, but below the year scale, suggests the arrival of winter low-energy conditions terminates the dominance for most of the year of the self-intensifying loop of evapotranspiration in semi-arid environments.

475

The bottom of Fig. 8c shows the sequence under low-energy conditions when evapotranspiration no longer outweighs the inhibiting of soil moisture and especially rainfall. This implies that the shift between a long period of interactions dominated by evapotranspiration (upper sequence of Fig. 8c) and a short period of interactions controlled by rainfall and soil moisture (lower sequence of Fig. 8c) can happen when radiation, as major driver of evapotranspiration, depletes during the low-energy period of

480   winter. However, additional processes may be of influence, such as the well-known atmospheric patterns of NAO or WeMO (Barnston and Livezey, 1987, Conte et al., 1989) or the oceanic ones like AMO (Kerr, 2000). The multiple periods showing neither prevalent positive nor negative correlations between indices indicate loss of linear interaction. A source of non-linearity is vegetation. Plants can control evapotranspiration and soil moisture in adaptation to water stress in complex manners that depend more on the type of vegetation (Katul et al., 2012) than in the evapotranspiration or soil moisture status. Plant impact both the

485   ETDI and SMDI because interactions of vegetation integrate the status of the atmospheric and the land-surface variables (Peters, Rundquist, & Wilhite, 1991). In the Mediterranean environment of this study, the quick response to drought of rainfed crops and sclerophyll vegetation and the lagged response of other vegetation types (Vicente-Serrano et al., 2019) may obscure interpreting the links between rainfall, evapotranspiration and soil moisture.

6.3 The value of remote sensing and land-surface model's estimates

490   The RS and LSM results of the lag analysis of the ETDI – SPI interactions show consistently comparable results in contrast to the remarkable disagreement between RS and LSM for the SMDI - SPI interaction. Results of SMDI obtained with the LSM show substantially lower correlations than the ones of RS, while also differing in the timing of the clusters of correlation. We expected the opposite, that the LSM, as being simpler than reality, has stronger SPI – ETDI - SMDI correlations than the RS dataset. We assume the implicit accumulation of uncertainties of modelling (Rodriguez-Iturbe et al., 1991), partly inherited from inputs but

495   also from LSM structure, cause the decrease of correlations. This is particularly true for soil moisture, a variable integrating exchanges between climate, soil and vegetation (Rodriguez-Iturbe et al., 2001). Secondly, this is an offline simulation, where the atmosphere (SAFRAN) is forcing the land-surface (SURFEX-ISBA), without and explicit feedback, because SURFEX-ISBA does not influence back SAFRAN. SAFRAN estimates real conditions by ingesting observations, so the feedback is implicit in results, which may be insufficient to represent reality. Thirdly, the model itself does not consider important processes like the interactive

500   response of vegetation. ISBA has an interactive vegetation module (ISBA-A-gs), but Mediterranean vegetation can be particularly challenging for it. We expect to test the capabilities of interactive modelling vegetation in a follow-up study. Uncertainties of ISBA with vegetation have also roots in the use of ECOCLIMAP2 database, which shows inaccuracies of cover type and LAI. ECOCLIMAP assumes the maximum/minimum LAI occur in June/February in contrast with the early spring and autumn LAI maximums characteristic of the Mediterranean environment (Queguiner et al., 2011). All in all, the differences between LSM and

505   RS dataset are already an important result to improve the LSM, and useful insight on the use of offline LSM drought simulations.

        Our results positively verify that RS represents an effective tool to overcome the problem of sparsely observed soil moisture or evapotranspiration, whose crucial role on drought evolution require high resolution data similarly to precipitation (AghaKouchak and Nakhjiri, 2012). Including high-res evapotranspiration products from MODIS (MOD16A2) and soil moisture from SMOS

510   missions (SMOS1km) together with the distributed rainfall reanalysis data allows dedicated interpretation of the interactions between these two drought-relevant variables and rainfall, and their role in the water balance of the land-surface interface (Dai, 2011). Especially for evapotranspiration, the maps and series of LSM SURFEX-ISBA are comparable of those of RS, which supports the reliability of LSM despite their limited capability in arid regions (De Kauwe et al., 2015).

515   The temporal and spatial patterns of the anomalies are overly identified both by RS and the LSM model. The RS data seems able to capture a more complex scheme of interactions than the LSM model, despite the intrinsic data issues of the RS sensors and the performance of the algorithms used to generate the products. Conversely, the LSM seems sensitive to uncertainties from input data, especially surface properties, and the offline forcing. Either way, uncertainties are causes of major concern in the lag analysis

520 where they can alter the correlations between indices and obscure the interpretation of the interactions. These aspects together with the complex response of vegetation to semi-arid environments can be critical to improve evapotranspiration and soil moisture estimates (Ukkola et al., 2016). Solving these inaccuracies would increase the value of RS and LSM estimates. This study exemplifies the potential of high-resolution RS and LSM products for a wide range of applications, such as drought analysis.

7 Conclusions and perspectives

The analysis of droughts in the Ebro basin using dedicated evapotranspiration and soil moisture drought indices based on high-525 resolution data from MOD16A2, SMOS1km and the LSM SURFEX-ISBA provide the following insights.

The monthly scale commonly adopted for drought evaluation (e.g., SPI-3) may overlook the quick evolution of drought from an agricultural and environmental perspective, especially in the high-energy climates of the Mediterranean basin where the anomalies of rainfall, evapotranspiration and soil moisture can vary in a matter of days. ETDI shows the strongest response at a weekly scale while it remains also influential in the mid-term. SMDI can also quickly evolve with anomalies of evapotranspiration and 530 particularly with lasting anomalies of rainfall. The weekly scale is advantageous to describe trends and shifts in the evolution of the indices and to identify disregarded interactions such as the preceding influence of ETDI on SPI.

The ETDI and SMDI indices, together with the SPI adapted to the weekly scale, allow to track the evolution of the anomalies of evapotranspiration, soil moisture and rainfall, as well as their interactions driving water anomalies in the region. There is great 535 consistency between time series of ETDI, SMDI and SPI. Lag analysis between these indices clarifies the interactions between anomalies on different levels of the surface-atmosphere system, information that is neglected when using multivariable indices. The lag analysis also identifies sequences of interactions defining reinforcing or inhibiting feedbacks. Evapotranspiration dominates the water balance of the Iberian semi-arid climate especially during high-energy periods. This dominance frequently exceeds the controlling action of rainfall and soil moisture, inducing the reinforcing dry loop. In view of the relevance of 540 evapotranspiration, heat waves further fueling dry events deserve further attention. The weak influence of soil moisture on subsequent evapotranspiration and rainfall limits its capability to control the propagation of the anomalies.

RS datasets of MOD16A2 and SMOS-1km accurately estimate the temporal and spatial anomalies in the basin. Evapotranspiration from the LSM SURFEX-ISBA closely resemble the RS one of MOD16A2. Results differ substantially between SMOS1km and 545 SURFEX-ISBA estimates of soil moisture. RS uncertainties arise mainly from data gaps. Land-surface model's estimates can extend the evaluation of soil moisture beyond the surface towards the root zone, but face notable challenges from offline simulation neglecting feedbacks, as well as from the quality of input data that defines surface characteristics. RS outcompetes the LSM on the ability to integrate information about challenging processes, such as the vegetation dynamics. Assimilation seems the way forward to integrate the best aspects of both kinds of data. For as long as ground-based observations remain sparse, RS and LSM represent 550 effective tools to assess the water anomalies of the land-atmosphere system and their interaction mechanisms.

References

555 AghaKouchak, A., and Nakhjiri, N.: A near real-time satellite-based global drought climate data record, Environ. Res. Lett.7(4), 044037, doi: 10.1088/1748-9326/7/4/044037, 2012.

AghaKouchak, A., Farahmand, A., Melton, F. S., Teixeira, J., Anderson, M. C., Wardlow, B. D., and Hain, C. R.: Remote sensing of drought: Progress, challenges and opportunities, Rev. Geophys., 53(2), 452-480, doi: 10.1002/2014RG000456, 2015.

Avissar, R., and Pielke, R. A.: A parameterization of heterogeneous land surfaces for atmospheric numerical models and its impact
560 on regional meteorology, Mon. Wea. Rev 117(10), 2113-2136, doi: 10.1175/1520-0493(1989)117<2113:APOHLS>2.0.CO;2,1989

Barella-Ortiz, A., and Quintana-Seguí, P. Evaluation of drought representation and propagation in regional climate model simulations across Spain, Hydrol. Earth Syst. Sci, 23(12), 5111-5131, doi: 10.5194/hess-23-5111-2019, 2019.

Barker, L.J., Hannaford, J., Chiverton, A., and Svensson, C.: From meteorological to hydrological drought using standardized
565 indicators, Hydrol. Earth Syst. Sci. Disc., 12(12):12,827–12,875, doi:10.5194/hessd-12-12827-2015, 2015.

Barnston, A. G., and Livezey, R. E.: Classification, Seasonality and Persistence of Low-Frequency Atmospheric Circulation Patterns, Mon. Wea. Rev., 115, 1083–1126, doi: 10.1175/1520-0493(1987)115<1083:CSAPOL>2.0.CO;2, 1987.

Bartalis, Z., Wagner, W., Naeimi, V., Hasenauer, S., Scipal, K., Bonekamp, H., ... and Anderson, C.: Initial soil moisture retrievals from the METOP-A Advanced Scatterometer (ASCAT), Geophys. Res. Lett., 34(20), doi: 10.1029/2007GL031088, 2007.

570 Beck, H.E., Zimmermann, N.E., McVicar, T.R., Vergopolan, N., Berg, A., and Wood, E.F.:Present and future Köppen-Geiger climate classification maps at 1-km resolution, Sci. Data, 5:180214, doi: 10.1038/sdata.2018.214, 2018.

Bisselink, B., and Dolman, A. J.: Precipitation recycling: Moisture sources over Europe using ERA-40 data, J. Hydrometeorol., 9(5), 1073-1083, doi: 10.1175/2008JHM962.1, 2008.

Boone, A., Calvet, J.C., and Noilhan, J.: Inclusion of a Third Soil Layer in a Land Surface Scheme Using the Force–Restore
575 Method, J. Appl. Meteorol., 38(11): 1611–1630, doi: 10.1175/1520-0450, 1999.

Brubaker, K. L., and Entekhabi, D.: Analysis of feedback mechanisms in land-atmosphere interaction, Water Resour. Res., 32(5), 1343-1357, doi: 10.1029/96WR00005, 1996.

Conte, M., Giuffrida, A., and Tedesco, S.: Mediterranean Oscillation: Impact on Precipitation and Hydrology in Italy, In Conference on Climate and Water, (Vol. 1), 1989.

580 Dai, A.: Drought under global warming: a review, Wiley Interdiscip. Rev. Clim. Change, 2(1), 45-65, doi: 10.1002/wcc.81, 2011.

Dasari, H. P., Pozo, I., Ferri-Yáñez, F., and Araújo, M. B.: A regional climate study of heat waves over the Iberian Peninsula, Atmospheric and Climate Sciences, 4(05), 841, doi: 10.4236/acs.2014.45074, 2014.

David, C. H., Habets, F., Maidment, D. R., and Yang, Z. L.: RAPID applied to the SIM-France model, Hydrol. Process., 25(22), 3412-3425, doi: 10.1002/hyp.8070, 2011.

585 Decharme, B., Boone, A., Delire, C., and Noilhan, J.: Local evaluation of the Interaction between Soil Biosphere Atmosphere soil multilayer diffusion scheme using four pedotransfer functions, J. Geophys. Res. Atmos., 116(D20), doi: 10.1029/2011JD016002, 2011.

De Kauwe, M. G., Zhou, S. X., Medlyn, B. E., Pitman, A. J., Wang, Y. P., Duursma, R. A., and Prentice, I. C.: Do land surface models need to include differential plant species responses to drought? Examining model predictions across a mesic-xeric gradient
590 in Europe, Biogeosciences, 12(24), 7503-7518, doi: 10.5194/bg-12-7503-2015, 2015.

Durand, Y., Giraud, G., Brun, E., Merindol, L. and Martin, E.: A computer-based system simulating snowpack structures as a tool for regional avalanche forecasting, J. Glaciol., 45, 469–484. ESPERE, cited 2006: Climate encyclopedia—Food and climate, doi: 10.3189/S0022143000001337, 1999.

595   Entekhabi, D., Njoku, E. G., O'Neill, P. E., Kellogg, K. H., Crow, W. T., Edelstein, W. N., ... and Kimball, J.: The soil moisture active passive (SMAP) mission, Proc. IEEE, 98(5), 704-716, doi: 10.1109/JPROC.2010.2043918, 2010.

Escorihuela, M. J., and Quintana-Seguí, P.: Comparison of remote sensing and simulated soil moisture datasets in Mediterranean landscapes, Remote Sens. Enviro., 180, 99-114, doi: 10.1016/j.rse.2016.02.046, 2016.

Escorihuela, M. J., Merlin, O., Stefan, V., Moyano, G., Eweys, O. A., Zribi, M., ... and Ghaout, S.: SMOS based high resolution soil moisture estimates for desert locust preventive management, Remote Sens. Appl.: Soc. Environ., 11, 140-150, doi:
600   10.1016/j.rsase.2018.06.002, 2018.

Farahmand, A., and AghaKouchak, A.: A generalized framework for deriving nonparametric standardized drought indicators, Adv. Water Resour., 76, 140-145, doi: 10.1016/j.advwatres.2014.11.012, 2015.

Faroux, S., Kaptué Tchuenté, A. T., Roujean, J. L., Masson, V., Martin, E., and Moigne, P. L.: ECOCLIMAP-II/Europe: A twofold database of ecosystems and surface parameters at 1 km resolution based on satellite information for use in land surface,
605   meteorological and climate models, Geosci. Model. Dev., 6(2), 563-582, doi: 10.5194/gmd-6-563-2013, 2013.

Gimeno, L., Nieto, R., Trigo, R. M., Vicente-Serrano, S. M., and López-Moreno, J. I.: Where does the Iberian Peninsula moisture come from? An answer based on a Lagrangian approach, J. Hydrometeorol., 11(2), 421-436, doi: 10.1175/2009JHM1182.1, 2010.

Gudmundsson, L., Rego, F. C., Rocha, M., and Seneviratne, S. I.: Predicting above normal wildfire activity in southern Europe as a function of meteorological drought, Environ. Res. Lett., 9(8), 084008, doi: 10.1088/1748-9326/9/8/084008, 2014.
610   Habets, F., Boone, A., Champeaux, J.L., Etchevers, P., Franchistéguy, L., Leblois, E., Ledoux, E., Le Moigne, P., Martin, E., Morel, S., 20 Noilhan, J., Quintana-Seguí, P., Rousset-Regimbeau, F., and Viennot, P.: The SAFRAN-ISBA-MODCOU hydrometeorological model applied over France, J. Geophys. Res., 113, doi: 10.1029/2007JD008548, 2008.

Herrera-Estrada, J. E., Satoh, Y., and Sheffield, J.: Spatiotemporal dynamics of global drought, Geophys. Res. Lett., 44(5), 2254-2263, doi:10.1002/2016GL071768, 2017.
615   Hoerling, M., Eischeid, J., Perlwitz, J., Quan, X., Zhang, T., and Pegion, P.: On the increased frequency of Mediterranean drought, J. Clim., 25(6), 2146-2161, doi: 10.1175/JCLI-D-11-00296.1, 2012.

Hornacek, M., Wagner, W., Sabel, D., Truong, H. L., Snoeij, P., Hahmann, T., ... and Doubková, M.: Potential for high resolution systematic global surface soil moisture retrieval via change detection using Sentinel-1, IEEE J. Sel. Top. Appl. Earth Obs. Remote Sens., 5(4), 1303-1311, doi: 10.1109/JSTARS.2012.2190136, 2012.
620   Jiménez, M. A., Jaksic, F. M., Armesto, J. J., Gaxiola, A., Meserve, P. L., Kelt, D. A., and Gutiérrez, J. R.: Extreme climatic events change the dynamics and invasibility of semi-arid annual plant communities, Ecol. Lett, 14(12), 1227-1235, doi: 10.1111/j.1461-0248.2011.01693.x, 2011.

Katul, G. G., Oren, R., Manzoni, S., Higgins, C., and Parlange, M. B.: Evapotranspiration: a process driving mass transport and energy exchange in the soil-plant-atmosphere-climate system, Rev. Geophys., 50(3), doi: 10.1029/2011RG000366, 2012.
625   Kerr, R. A.: A North Atlantic Climate Pacemaker for the Centuries, Science, 288(5473), 1984–1985, doi: 10.1126/science.288.5473.1984, 2000.

Kerr, Y. H., Waldteufel, P., Wigneron, J. P., Delwart, S., Cabot, F., Boutin, J., ... and Juglea, S. E.: The SMOS mission: New tool for monitoring key elements ofthe global water cycle, Proc. IEEE, 98(5), 666-687, doi: 10.1109/JPROC.2010.2043032, 2010

Ledoux, E., Girard, G., De Marsily, G., Villeneuve, J. P., and Deschenes, J. : Spatially distributed modeling: conceptual approach,
630   coupling surface water and groundwater. In Unsaturated Flow in Hydrologic Modeling (pp. 435-454). Springer, Dordrecht, doi: 10.1007/978-94-009-2352-2_16, 1989.

Natural Hazards
and Earth System
Sciences
Discussions

Le Moigne, P., Besson, F., Martin, E., Boé, J., Boone, A., Decharme, B., Etchevers, P., Faroux, S., Habets, F., Lafaysse, M., Leroux, D., and Rousset-Regimbeau, F.: The latest improvements with SURFEX v8.0 of the Safran–Isba–Modcou hydrometeorological model for France, Geosci. Model Dev.,13(9), 3925–3946, doi: 10.5194/gmd-13-3925-2020, 2020.

635 López-Moreno, J. I., Zabalza, J., Vicente-Serrano, S. M., Revuelto, J., Gilaberte, M., Azorin-Molina, C., ... and Tague, C.: Impact of climate and land use change on water availability and reservoir management: Scenarios in the Upper Aragón River, Spanish Pyrenees, Sci. Total Environ., 493, 1222-1231, doi: 10.1016/j.scitotenv.2013.09.031, 2014.

Manning, C., Widmann, M., Bevacqua, E., Van Loon, A. F., Maraun, D., and Vrac, M.: Soil moisture drought in Europe: a compound event of precipitation and potential evapotranspiration on multiple time scales, J. Hydrometeorol., 19(8), 1255-1271,

640 doi: 10.1175/JHM−D−18−0017.1, 2018.

Martínez-Fernández, J., González-Zamora, A., Sánchez, N., Gumuzzio, A., and Herrero-Jiménez, C. M.: Satellite soil moisture for agricultural drought monitoring: Assessment of the SMOS derived Soil Water Deficit Index, Remote Sens. Environ., 177, 277-286, doi: 10.1016/j.rse.2016.02.064, 2016.

Masson, V., Le Moigne, P., Martin, E., Faroux, S., Alias, A., Alkama, R., ... and Brousseau, P.: The SURFEXv7. 2 land and ocean

645 surface platform for coupled or offline simulation of earth surface variables and fluxes, Geosci. Model Dev., 6, 929–960, doi: 10.5194/gmd-6-929-2013, 2013.

Mauser, W., and Schadlich, S.: Modelling the Spatial Distribution of Evapotranspiration Using Remote Sensing Data and PROMET, J. Hydrology, 213, 250, 267, doi: 10.1016/S0022-1694(98)00228-5, 1998.

McKee, T.B., Doesken, N.J. and Kleist., J.: The relationship of drought frequency and duration to time scale. In: Proceedings of

650 the Eighth Conference on Applied Climatology, Anaheim, California, 17–22 January 1993, Boston, American Meteorological Society, 179–184, 1993.

Merlin, O., Rudiger, C., Al Bitar, A., Richaume, P., Walker, J. P., and Kerr, Y. H.: Disaggregation of SMOS soil moisture in Southeastern Australia, IEEE Trans. Geosci. Remote Sens., 50(5), 1556-1571, doi: 10.1109/TGRS.2011.2175000, 2012.

Merlin, O., Escorihuela, M. J., Mayoral, M. A., Hagolle, O., Al Bitar, A., and Kerr, Y.: Self-calibrated evaporation-based

655 disaggregation of SMOS soil moisture: An evaluation study at 3 km and 100 m resolution in Catalunya, Spain, Remote Sens. Environ., 130, 25-38, doi: 10.1016/j.rse.2012.11.008, 2013.

Miralles, D. G., Gentine, P., Seneviratne, S. I., and Teuling, A. J.: Land–atmospheric feedbacks during droughts and heatwaves: state of the science and current challenges, Ann. N. Y. Acad. Sci., 1436(1), 19, doi: 10.1111/nyas.13912, 2019.

MMA: Libro Blanco del Agua en España. Spanish Ministry of Environment (MMA), 2000.

660 Molero, B., Merlin, O., Malbéteau, Y., Al Bitar, A., Cabot, F., Stefan, V., ... and Jackson, T. J.: SMOS disaggregated soil moisture product at 1 km resolution: Processor overview and first validation results, Remote Sens. Environ., 180, 361-376, doi: 10.1016/j.rse.2016.02.045, 2016.

Mu, Q., Zhao, M., and Running, S. W.: MODIS global terrestrial evapotranspiration (ET) product (NASA MOD16A2/A3). Algorithm Theoretical Basis Document, Collection, 5, 2013.

665 Narasimhan, B., and Srinivasan, R.: Development and evaluation of Soil Moisture Deficit Index (SMDI) and Evapotranspiration Deficit Index (ETDI) for agricultural drought monitoring, Agric. For. Meteorol., 133(1-4), 69-88, doi: 10.1016/j.agrformet.2005.07.012, 2005.

Noilhan, J., and Mahfouf, J. F.: The ISBA land surface parameterisation scheme, Glob. Planet. Change., 13(1-4), 145-159, doi: 10.1016/0921-8181(95)00043-7, 1996.

670   Otkin, J. A., Anderson, M. C., Hain, C., Mladenova, I. E., Basara, J. B., and Svoboda, M.: Examining rapid onset drought development using the thermal infrared–based evaporative stress index, J. Hydrometeorol., 14(4), 1057-1074, doi: 10.1175/JHM-D-12-0144.1, 2013.

Otkin, J. A., Anderson, M. C., Hain, C., and Svoboda, M.: Using temporal changes in drought indices to generate probabilistic drought intensification forecasts, J. Hydrometeorol., 16(1), 88-105, doi: 10.1175/JHM-D-14-0064.1, 2015

675   Pablos, M., Martínez-Fernández, J., Sánchez, N., and González-Zamora, Á.: Temporal and spatial comparison of agricultural drought indices from moderate resolution satellite soil moisture data over Northwest Spain, Remote Sens., 9(11), 1168, doi: 10.3390/rs9111168, 2017.

Palmer, W. C.: Meterolological drought. U.S. Weather Bureau, Res. Pap. No. 45, 58 pp, 1965.

Peters, A. J., Rundquist, D. C., and Wilhite, D. A.: Satellite detection of the geographic core of the 1988 Nebraska drought, Agric.

680   For. Meteorol., 57(1-3), 35-47, doi: 10.1016/0168-1923(91)90077-4, 1991.

Queguiner, S., Martin, E., Lafont, S., Calvet, J.-C., Faroux, S., and Quintana-Seguí, P.: Impact of the use of a CO2 responsive land surface model in simulating the effect of climate change on the hydrology of French Mediterranean basins, Nat. Hazards Earth Syst. Sci., 11, 2803–2816, doi: 10.5194/nhess-11-2803-2011, 2011.

Quintana-Segui, P., Le Moigne, P., Durand, Y., Martin, E., Habets, F., Baillon, M., ... and Morel, S.: Analysis of near-surface

685   atmospheric variables: Validation of the SAFRAN analysis over France, J Appl. Meteorol. Climatol., 47(1), 92-107, doi:10.1175/2007JAMC1636.1, 2008.

Quintana-Seguí, P., Peral, M.C., Turco, M., Llasat, M.C., and Martin, E.: Meteorological Analysis Systems in North-East Spain: Validation of SAFRAN and SPAN, J. Environ. Inform., 27(2):116–130, doi:10.3808/jei.201600335, 2016.

Quintana-Seguí, P., Turco, M., Herrera, S., and Miguez-Macho, G.: Validation of a new SAFRAN-based gridded precipitation

690   product for Spain 25 and comparisons to Spain02 and ERA-Interim, Hydrol. Earth Syst. Sci., 21(4):2187–2201, doi: 10.5194/hess-21-2187- 2017, 2017.

Quintana-Seguí, P., Barella-Ortiz, A., Regueiro-Sanfiz, S., and Miguez-Macho, G.: The utility of land-surface model simulations to provide drought information in a water management context using global and local forcing datasets, Water Resour. Manag., 34(7), 2135-2156, doi: 10.1007/s11269-018-2160-9, 2020.

695   Ribeiro, A. F., Russo, A., Gouveia, C. M., and Páscoa, P.: Modelling drought-related yield losses in Iberia using remote sensing and multiscalar indices, Theor. Appl. Climatol., 136(1-2), 203-220, doi: 10.1007/s00704-018-2478-5, 2019.

Rodriguez-Iturbe, I., Entekhabi, D., and Bras, R. L.: Nonlinear dynamics of soil moisture at climate scales: 1. Stochastic analysis, Water Resour. Res., 27(8), 1899-1906, doi: 10.1029/91WR01035, 1991.

Rodriguez-Iturbe, I., Porporato, A., Laio, F., and Ridolfi, L.: Plants in water-controlled ecosystems: active role in hydrologic

700   processes and response to water stress: I. Scope and general outline, Adv. Water Resour., 24(7), 695-705, doi: 10.1016/S0309-1708(01)00005-7, 2001.

Rowntree, P. R., and Bolton, J. A.: Simulation of the atmospheric response to soil moisture anomalies over Europe, Q. J. R. Meteorol. Soc., 109(461), 501-526, doi: 10.1002/qj.49710946105, 1983.

Running, S. W., Mu, Q., Zhao, M., & Moreno, A.: MODIS Global Terrestrial Evapotranspiration (ET) Product (NASA

705   MOD16A2/A3) NASA Earth Observing System MODIS Land Algorithm. NASA: Washington, DC, USA, 2017.

Saini, Hargurdeep S., and Westgate, M. E.: Reproductive development in grain crops during drought. Advances in agronomy. Vol. 68. Academic Press. 59-96, doi: 10.1016/S0065-2113(08)60843-3, 1999.

Sánchez, N., González-Zamora, Á., Piles, M., and Martínez-Fernández, J.: A new Soil Moisture Agricultural Drought Index (SMADI) integrating MODIS and SMOS products: A case of study over the Iberian Peninsula, Remote Sens., 8(4), 287, doi: 10.3390/rs8040287, 2016.

710

Savenije, H. H.: The importance of interception and why we should delete the term evapotranspiration from our vocabulary, Hydrol. Process., 18(8), 1507-1511, doi: 10.1002/hyp.5563, 2004.

Scaini, A., Sánchez, N., Vicente-Serrano, S. M., and Martínez-Fernández, J. : SMOS-derived soil moisture anomalies and drought indices: a comparative analysis using in situ measurements, Hydrol. Process., 29(3), 373-383, doi: 10.1002/hyp.10150, 2015.

715 Schultz, K., Franks, S., and Beven, K.: TOPUP–A TOPMODEL based SVAT model to calculate evaporative fluxes between the land surface and the atmosphere, Version 1.1, Program documentation, 1998.

Seneviratne, S. I., Lüthi, D., Litschi, M., and Schär, C.: Land–atmosphere coupling and climate change in Europe, Nature, 443(7108), 205-209, doi: 10.1038/nature05095, 2006.

Seneviratne, S. I., Corti, T., Davin, E. L., Hirschi, M., Jaeger, E. B., Lehner, I., ... and Teuling, A. J.: Investigating soil moisture–

720 climate interactions in a changing climate: A review, Earth Sci. Rev., 99(3-4), 125-161, doi: 10.1016/j.earscirev.2010.02.004,.

Sepulcre-Canto, G., Horion, S. M. A. F., Singleton, A., Carrao, H., and Vogt, J.: Development of a Combined Drought Indicator to detect agricultural drought in Europe, Nat. Hazards Earth Syst. Sci., 12(11), doi: 10.5194/nhess-12-3519-2012, 2012.

Sousa, P. M., Trigo, R. M., Aizpurua, P., Nieto, R., Gimeno, L., and García Herrera, R.: Trends and extremes of drought indices throughout the 20th century in the Mediterranean, Nat. Hazards Earth Syst. Sci., 11(1), 33-51, doi: 10.5194/nhess-11-33-2011.

725 Teuling, A. J., Van Loon, A. F., Seneviratne, S. I., Lehner, I., Aubinet, M., Heinesch, B., ... and Spank, U.: Evapotranspiration amplifies European summer drought, Geophys. Res. Lett., 40(10), 2071-2075, doi: 10.1002/grl.50495, 2013.

Tigkas, D., and Tsakiris, G.: Early estimation of drought impacts on rainfed wheat yield in Mediterranean climate, Environ. Process., 2(1), 97-114, doi: 10.1007/s40710-014-0052-4, 2015.

Turco, M., and Llasat, M. C.: Trends in indices of daily precipitation extremes in Catalonia (NE Spain), 1951–2003, Nat. Hazards

730 Earth Syst. Sci., 11(12), 3213-3226, doi: 10.5194/nhess-11-3213-2011, 2011.

Ukkola, A. M., Pitman, A. J., Decker, M., De Kauwe, M. G., Abramowitz, G., Kala, J., and Wang, Y. P.: Modelling evapotranspiration during precipitation deficits: identifying critical processes in a land surface model, Hydrol. Earth Syst. Sci., 20(6), 2403-2419, doi: 10.5194/hess-20-2403-2016, 2016.

Van Loon, Anne F.: Hydrological drought explained. Wiley Interdiscip. Rev. Water, 2.4, 2015: 359-392, doi: 10.1002/wat2.1085,

735 2015.

Vicente-Serrano, S. M., González-Hidalgo, J. C., de Luis, M., and Raventós, J.: Drought patterns in the Mediterranean area: the Valencia region (eastern Spain), Clim. Res., 26(1), 5-15, doi: 10.3354/cr026005, 2004.

Vicente-Serrano, S. M.: Evaluating the Impact of Drought Using Remote Sensing in a Mediterranean, Semi-arid Region, Nat. Hazards, 40(1), 173–208, doi:10.1007/s11069-006-0009-7 , 2006.

740 Wagner, W., Blöschl, G., Pampaloni, P., Calvet, J. C., Bizzarri, B., Wigneron, J. P., and Kerr, Y.: Operational readiness of microwave remote sensing of soil moisture for hydrologic applications, Hydrol. Res., 38(1), 1-20, doi: 10.2166/nh.2007.029, 2007.

Watts, G., Christierson, B. von, Hannaford, J., and Lonsdale, K.: Testing the resilience of water supply systems to long droughts, J. Hydrol., 414-415, 255–267, doi: 10.1016/j.jhydrol.2011.10.038, 2012.

Zampieri, M., D'Andrea, F., Vautard, R., Ciais, P., de Noblet-Ducoudré, N., and Yiou, P. : Hot European summers and the role of

745 soil moisture in the propagation of Mediterranean drought, J. Clim., 22(18), 4747-4758, doi: 10.1175/2009JCLI2568.1, 2009.
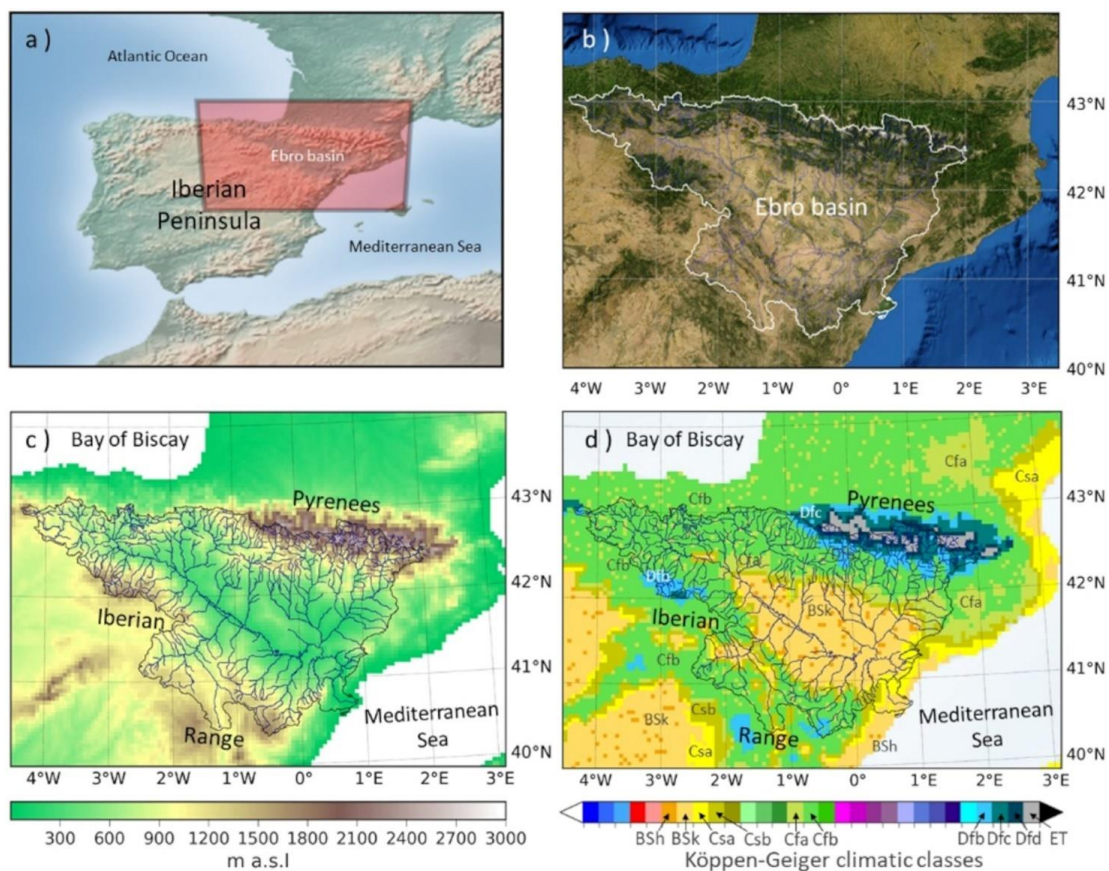
Figure 1: a) Ebro basin location in the Iberian Peninsula (OSM OpenTopoMap). b) Land cover of the basin describes a contrasted basin between the forested areas of the mountains and the steppes of the central depression (© ESRI satellite online maps, World Imagery, 2022). c) Altitudinal range of the basin (IGN ES/FR MDT25, CC-BY 4.0). D) Climatic classes present in the basin according to the climatic classification of Köppen-Geiger (from data of Beck et al. (2018)).

Pairs of indices	r Pearson correlation coefficient of the monthly time series (ETDIm, SMDIm, SPIm-i)		r Pearson correlation coefficient of the weekly time series (ETDIw, SMDIw, SPIw-i)	
	2010-2017	Dry periods	2010-2017	Dry periods
ETDI RS and ETDI LSM	**0.77**	**0.60**	**0.55**	**0.34**
SMDI RS and SMDI LSM	**0.27**	0.13	**0.19**	0.12
ETDI RS and SMDI RS	**0.58**	**0.50**	**0.50**	**0.46**
ETDI LSM and SMDI LSM	**0.32**	**0.43**	**0.21**	0.18
SPIm-1/SPIw-4 and ETDI RS	**0.39**	0.23	**0.57**	**0.30**
SPIm-1/SPIw-4 and ETDI LSM	**0.51**	**0.37**	**0.68**	**0.49**
SPIm-1/SPIw-4 and SMDI RS	**0.42**	0.52	**0.57**	**0.57**
SPIm-1/SPIw-4 and SMDI LSM	**0.45**	**0.59**	**0.33**	**0.25**
SPIm-3/SPIw-13 and ETDI RS	**0.62**	**0.42**	**0.63**	**0.32**
SPIm-3/SPIw-13 and ETDI LSM	**0.8**	**0.67**	**0.74**	**0.47**
SPIm-3/SPIw-13 and SMDI RS	**0.61**	**0.41**	**0.51**	**0.36**
SPIm-3/SPIw-13 and SMDI LSM	**0.41**	0.32	**0.21**	**0.29**
SPIm-6/SPIw-26 and ETDI RS	**0.72**	**0.45**	**0.57**	**0.21**
SPIm-6/SPIw-26 and ETDI LSM	**0.78**	**0.39**	**0.60**	**0.30**
SPIm-6/SPIw-26 and SMDI RS	**0.58**	0.19	**0.40**	**0.40**
SPIm-6/SPIw-26 and SMDI LSM	**0.30**	0.17	**0.16**	0.02
SPIm-12/SPIw-52 and ETDI RS	**0.81**	**0.75**	**0.48**	**0.31**
SPIm-12/SPIw-52 and ETDI LSM	**0.71**	**0.53**	**0.45**	**0.16**
SPIm-12/SPIw-52 and SMDI RS	**0.63**	**0.40**	**0.43**	**0.39**
SPIm-12/SPIw-52 and SMDI LSM	**0.24**	0.22	**0.15**	-0.03

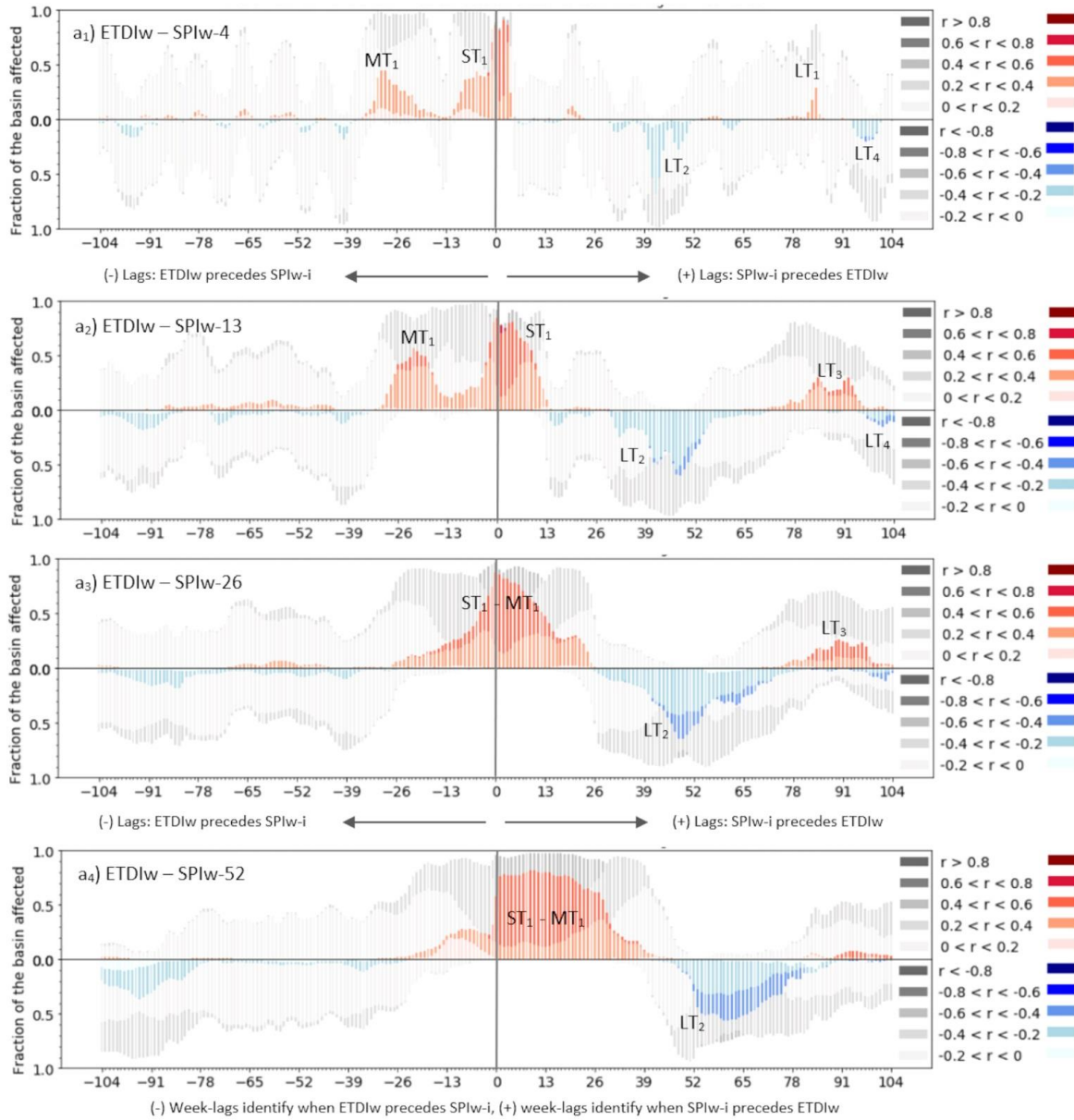* Dry periods considered when SPI<0, ETDI<0, SMDI<0

Table 1: Significant (in bold) correlation coefficients considering p-values=0.05 for pairs of indices at monthly and weekly scale, for the period 2010-2017 of the SPI-i, ETDI and SMDI series, including results for the subset of dry periods in the series.
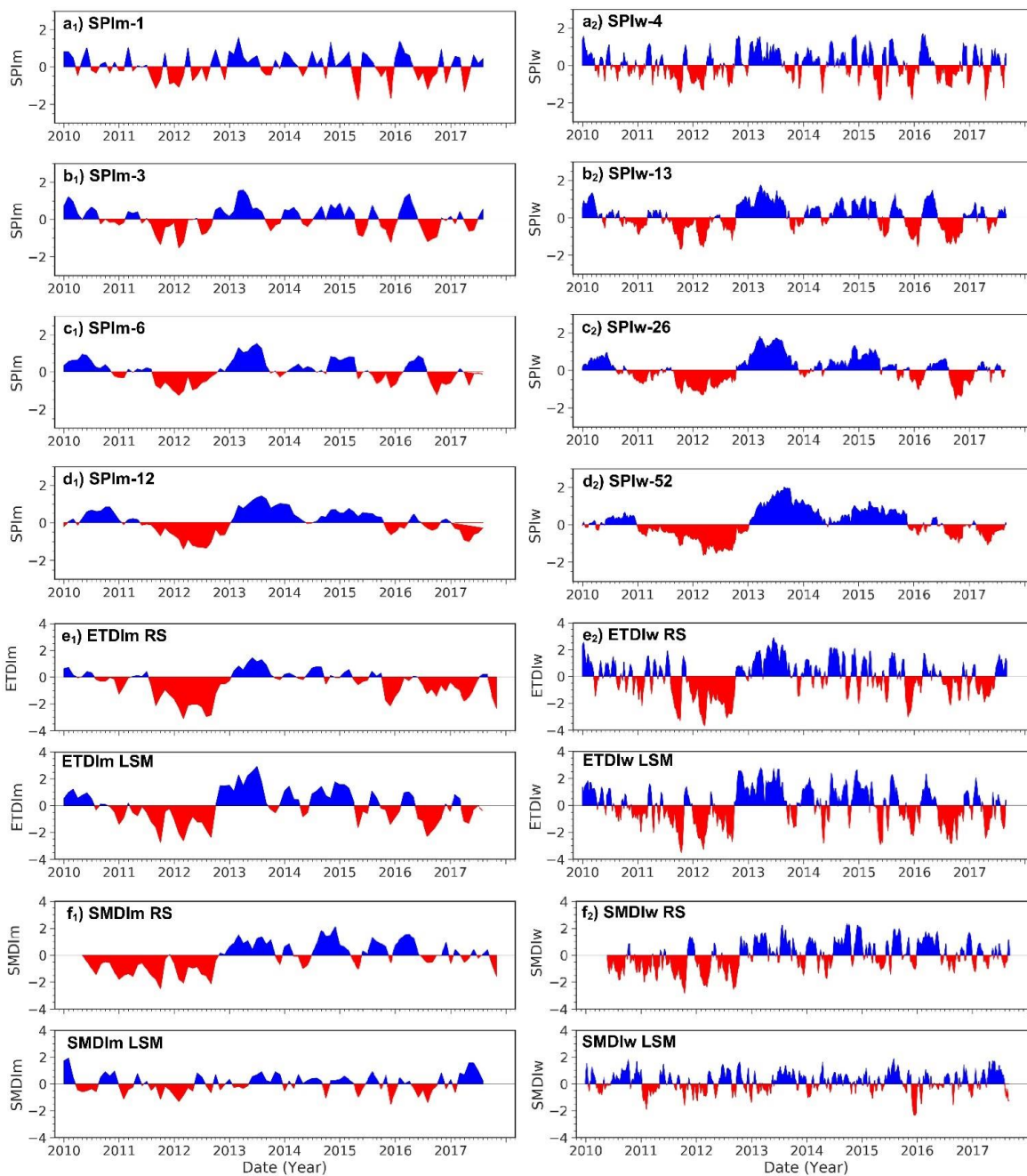
Figure 2: Time series of SPI, ETDI and SMDI indices at monthly scale (left column of subplots identified with sub-index 1) and weekly scale (right column of subplots identified with sub-index 2). a) to d) correspond to SPIm-1, SPIm-3, SPIm-6 and SPIm-12, e) and f) display the temporal evolution of the ETDI and SMDI. These ones show two rows corresponding to the series based on RS and LSM data. Red /blue color represents dry /wet periods. Periods of drought occur when SPI<0, ETDI>0, SMDI<0.
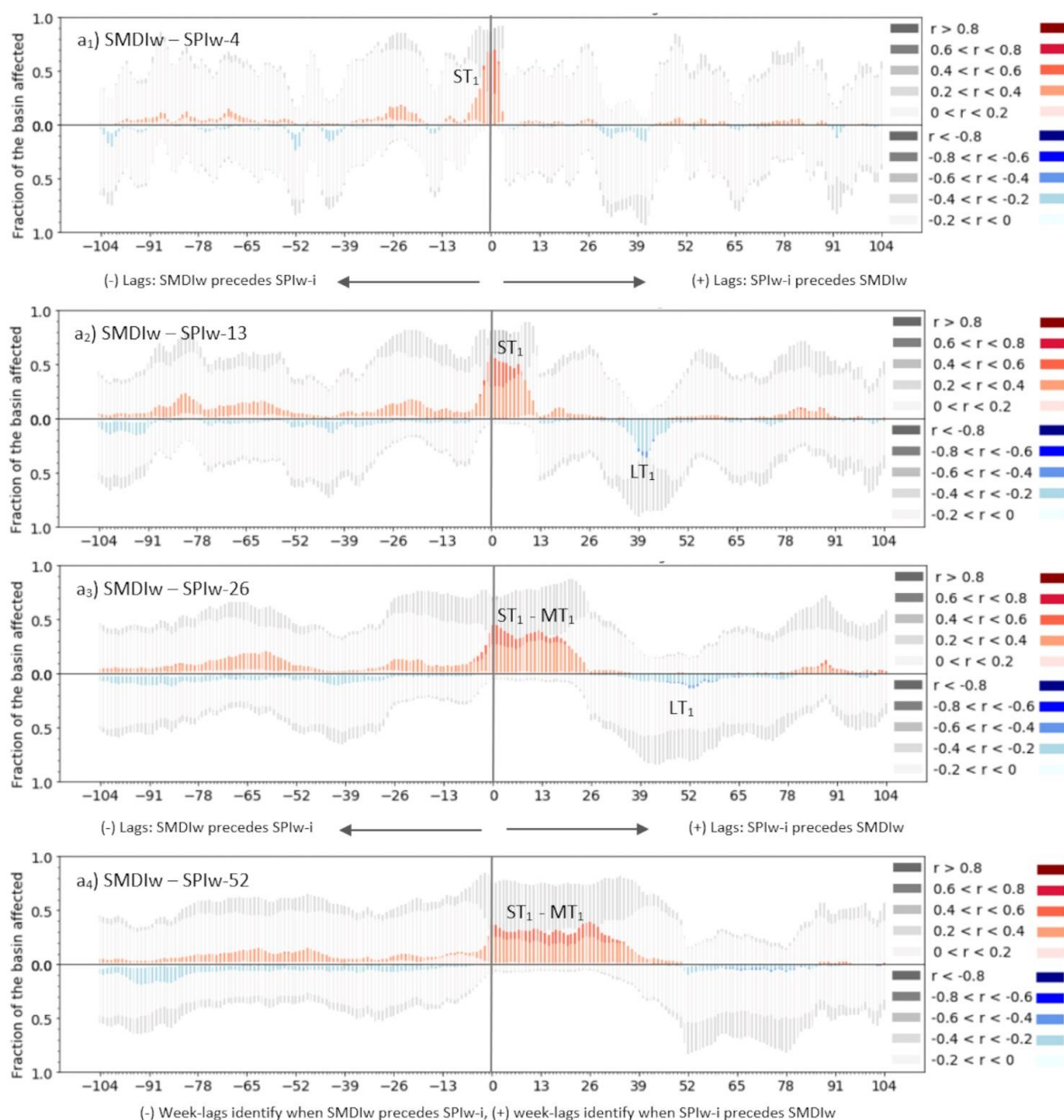
Figure 3: Lag plots of SPI-1, SPI-3, SPI-6 and SPI-12 (expressed as SPIw-4, 13, 26, and 52 weeks respectively) with remote sensing (RS) ETDIw index at weekly scale for the period 2010-2017. Lags are calculated for the -104 leading and +104 lagged time steps of ETDIw in reference to the SPIw-i. The height of the bars of the plot indicates the area of the basin affected by non-significant (grey scale) or significant (coloured scale) correlations. The saturation of the colored scale indicates the magnitude of the significant positive (red) or negative (blue) Pearson correlation coefficient of SPIw-i and ETDIw.

Natural Hazards
and Earth System
Sciences
Discussions

Open Access

EGU
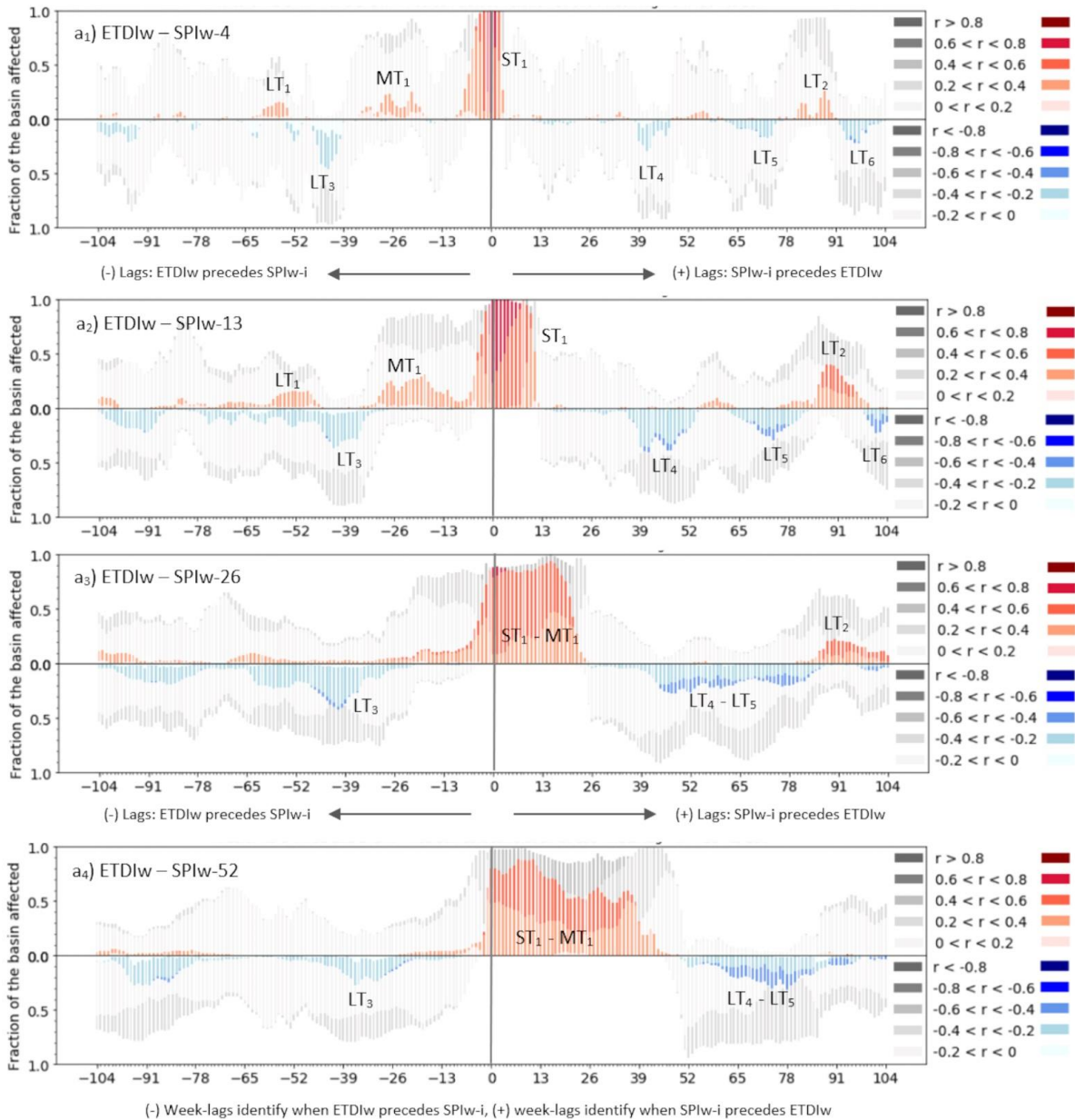
Figure 4: Lag plots of SPI-1, SPI-3, SPI-6 and SPI-12 (expressed as SPIw-4, 13, 26, and 52 weeks respectively) with land-surface model

775   **(LSM) ETDIw index at weekly scale for the period 2010-2017. Lags are calculated for the -104 leading and +104 lagged time steps of ETDIw in reference to the SPIw-i. The height of the bars of the plot indicates the area of the basin affected by non-significant (grey scale) or significant (coloured scale) correlations. The saturation of the colored scale indicates the magnitude of the significant positive (red) or negative (blue) Pearson correlation coefficient of SPIw-i and ETDIw.**

Figure 5: Lag plots of SPI-1, SPI-3, SPI-6 and SPI-12 (expressed as SPIw-4, 13, 26, and 52 weeks respectively) with remote sensing (RS) SMDIw index at weekly scale for the period 2010-2017. Lags are calculated for the -104 leading and +104 lagged time steps of SMDIw in reference to the SPIw-i. The height of the bars of the plot indicates the area of the basin affected by non-significant (grey scale) or significant (colored scale) correlations. The saturation of the colored scale indicates the magnitude of the significant positive (red) or negative (blue) Pearson correlation coefficient of SPIw-i and SMDIw.
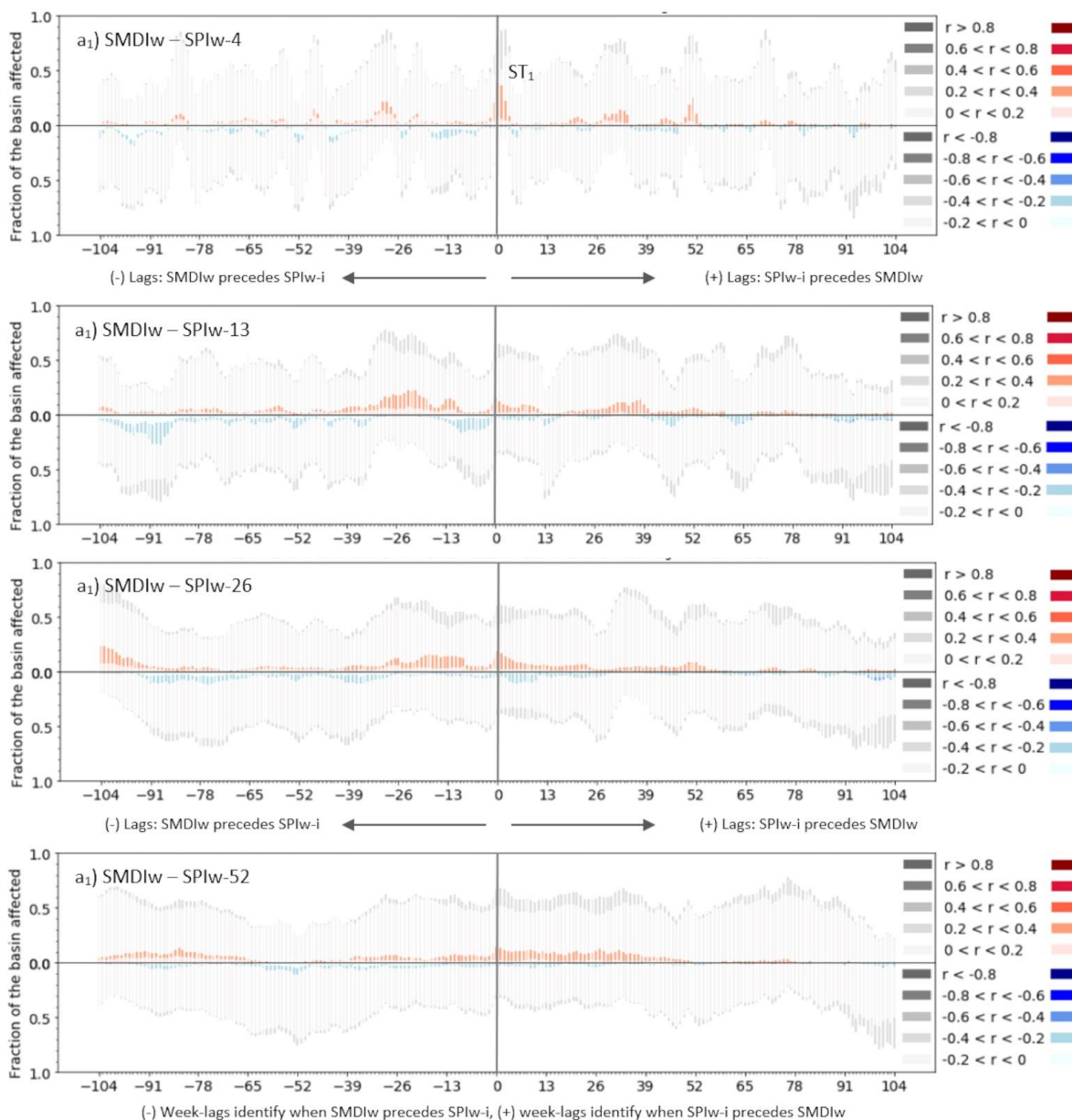
Figure 6: Lag plots of SPI-1, SPI-3, SPI-6 and SPI-12 (expressed as SPIw-4, 13, 26, and 52 weeks respectively) with land-surface model (LSM) SMDIw index at the weekly scale for the period 2010-2017. Lags are calculated for the -104 leading and +104 lagged time steps of SMDIw in reference to the SPIw-i. The height of the bars of the plot indicates the area of the basin affected by non-significant (grey scale) or significant (colored scale) correlations. The saturation of the colored scale indicates the magnitude of the significant positive (red) or negative (blue) Pearson correlation coefficient of SPIw-i and SMDIw.

790
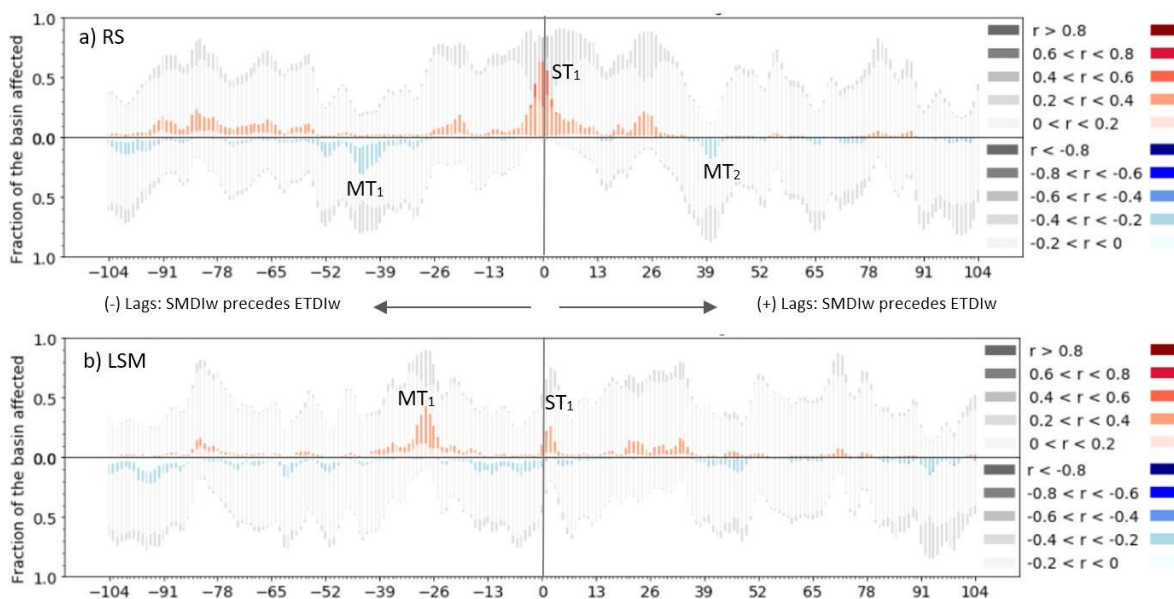
Figure 7: Lag plots of ETDIw – SMDIw at weekly time scale in the period 2010-2017 for a) RS data and b) LSM data. Lags are calculated for the -104 leading and +104 lagged time steps of SMDIw in reference to the SPIw-4. The five levels of red and blue indicate the positive (red) or negative (blue) Pearson correlation coefficient between the ETDIw and the SMDIw for each time step (lead or lag time step). The height of the bars of the plot indicates the area of the basin affected by that level level of r Pearson values.
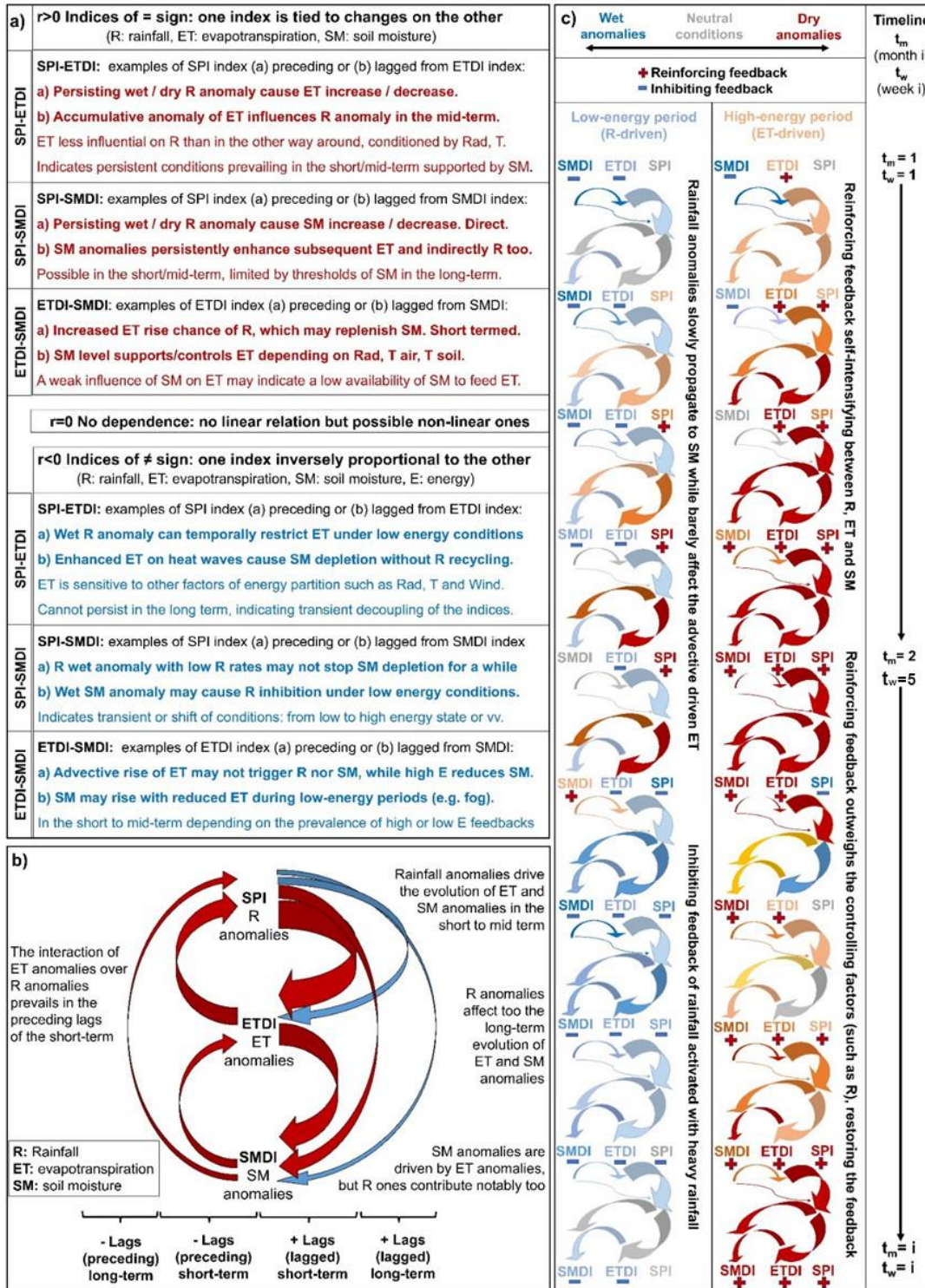
800

Figure 8: (a) Interpretation of the correlations between SMDI-SPI, ETDI-SPI and SMDI-ETDI indices. The r>0 box exemplifies positive correlations between the indices (positive correlations of red arrows in b)) while the r<0 box defines the negative ones (negative

Natural Hazards
and Earth System
Sciences

Open Access

EGU

Discussions

805   **correlations of blue arrows in b)). (b) Summary of the annual magnitude and timing of the interactions. Red arrows represent positive correlations while blue arrows the negative ones. Arrow width represents the magnitude of the correlation. Arrow direction determines the direction of the interaction. The timeline in the bottom indicates the scale of the interactions ranging from short-term to long-term. (c) Sequences of prevalent reinforcing (upper) and inhibiting (lower) conditions alternating during the annual cycle based on the scheme of interactions described in a) and b). The upper sequence is the self-intensifying loop driven by evapotranspiration under high-energy conditions. The lower sequence displays the inhibiting role of rainfall / soil moisture under low-energy conditions.**